Stabilising a Ring Dye Laser to Iodine Transitions

for Quantum Computing and Photon Echoes

Master's thesis
by
Robert Saers

Lund Reports on Atomic Physics, LRAP-282
Lund, March 2002

Abstract

Saturation spectroscopy of Iodine is used to lock the frequency of a Coherent 699-21 Ring Dye laser. Without an external reference the laser frequency drifts several tens of MHz per hour. With the system presented in this thesis the drift has been reduced to a maximum of $\pm$1MHz.

Theoretical description of saturation spectroscopy and hole burning is given and the experiments are presented.

In preparation for future experiments in quantum computing hole burning in rare-earth-ion-doped crystals and broadening of the hole by excitation of ions at different intervals have also been studied in this master's thesis.

Contents

Chapter 1

Introduction

Frequency stability is an essential property of a laser. A major reason for the breakthrough of lasers was their capacity as single frequency emitters of coherent light.

The first lasers were fixed to a certain frequency, determined by the position of the energy levels in the materials used as amplification media in the laser. Non frequency-tuneable lasers are still important but are often used to pump tuneable lasers. The Coherent 699 Dye laser is such a tuneable laser. The amplification media consists of a dye. The complex structure of the dye molecules results in a broad emission spectrum. Introducing an adjustable frequency filter inside the cavity gives a narrow-band and tunable laser, a very powerful tool in e.g. atomic physics.

1.1 Single Photon Interference and Quantum Computers

In the Photon Echo group, at the Division of Atomic Physics at Lund Institute of Technology, experiments are carried out concerning among other things single photon interference and quantum computing. For both these areas stable lasers are needed that can operate in different wavelength regions. Two Coherent 699 Dye laser systems pumped by one Argon Ion pumped, and one Millennia Diode pumped $Nd:YVO_4$ laser, are available. The dye lasers have built in frequency stabilisation systems, but these tend to drift in frequency over long time scales. The bandwidth of the laser is specified to 1 MHz and the actual frequency drift of the lasers used in the lab has been examined by Tomas Christiansson [1]. As seen in figure 1.1 the laser frequency drifts several tens of MHz/hour and cannot be regarded as frequency stable if MHz precision over long time is needed.

1.1.1 Single Photon Interference

The single photon interference experiment is carried out by Nicklas Ohlsson [2]. The aim of the experiment is to create a photon echo using single photons.

When incoming light illuminates two slits it becomes spectrally, and spatially, separated. If a screen is placed after the slits, different wavelengths will

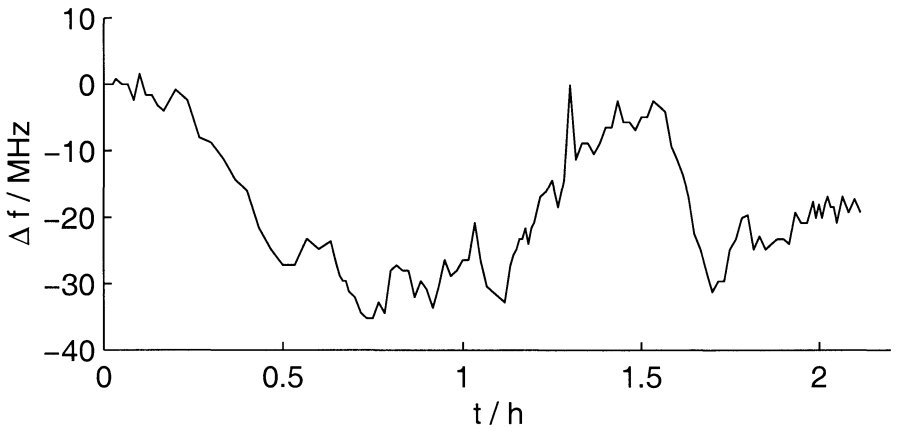

Figure 1.1: The frequency drift of the Coherent 699 Dye laser versus time. Many experiments require better stability. Sub-MHz frequency stability is essential in quantum computing experiments performed at Lund Institute of Technology.

interfere at different positions on the screen. Creating a photon echo is an experiment, similar to the two slits, consisting of incoming laser pulses. The first resonant excitation pulse puts ions, in e.g. a crystal, in a superposition of a ground and excited state. Right after the first pulse the ions radiate in phase. As they all have slightly different frequencies the phases develop differently for different ions. When sending in a second pulse of the same frequency as the first, an interference pattern is created in the frequency plane. Ions that are radiating in phase with the second pulse are excited and those out of phase are de-excited, as seen in figure 1.2. When a third pulse is sent in at a later time, it interferes with the interference pattern created by the first two pulses. Individual ions will radiate at their different resonance frequencies with different amplitudes but after a time equal to the separation between pulse 1 and 2 the radiation from all the ions will be in phase. At this time an echo is emitted. See figure 1.2 and 1.3. The important similarities between the double slit and the photon echo experiment lies within the distributions. In the traditional double slit experiment the light will be redistributed in space and in the photon echo case the light pulse will be redistributed in time.

In the single photon experiment the pulse intensity is attenuated to less than one photon per pulse. By measuring the intensity of the pulses, the photon rate can be adjusted to 0,5-1 photons per pulse train. With this low photon density there is a small probability of having two photons coming through in the same pulse train. If an echo is detected, single photon interference is proved. Since it is very difficult to detect such small signals, many pulse pairs containing one photon are sent in. After accumulating the grating with a sufficiently large number of pulses, an intensive readout pulse is sent in (third pulse in figure 1.3). The results of all the pairs sent in are detected together and at the same time.

To be able to accumulate over a long time a laser, stable to within 10 MHz for a period of time of the order of tens of minutes, is needed. This stability is normally not obtained with the standard laser used.

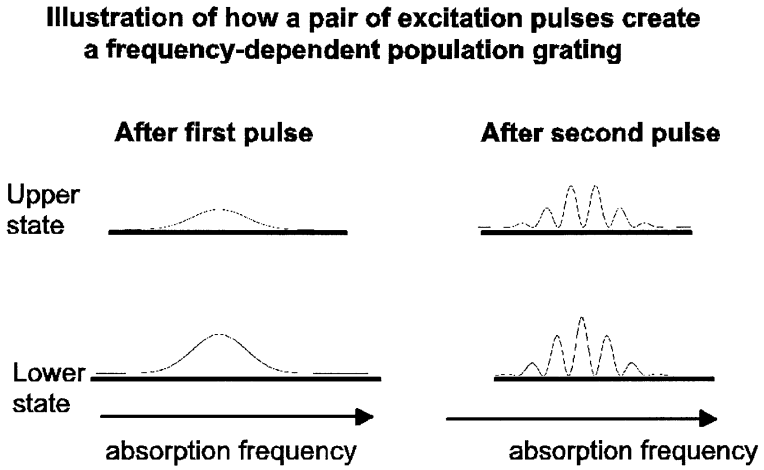

Figure 1.2: The population distributions between the upper and the lower states as a function of absorption frequency during the creation of a photon echo.

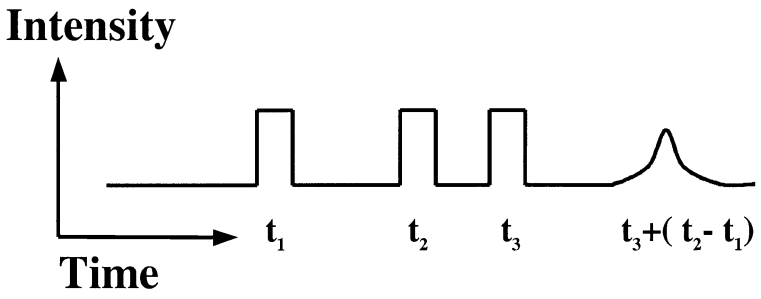

Figure 1.3: Timing of the pulses used to make a standard photon echo experiment.

1.1.2 Quantum Computing

A quantum computer relies on the two fundamental properties of *superposition* and *entanglement.*

Superposition

In quantum mechanics calculations are done on probabilities. A system with for example 2 energy levels has a certain probability of being in one or the other level. By interacting with the system the probabilities can be changed. The state of the system will not be well defined until a measurement is carried out, i.e. the state collapses into one of its eigenstates.

The system can be described by

$$|\psi\rangle = a\,|\psi_a\rangle + b\,|\psi_b\rangle\,.$$

Measuring on the system will give the state $|\psi_a\rangle$ with the probability $|a|^2$ and $|\psi_b\rangle$ with $|b|^2$.

The major difference between classical and quantum computers is that in the classic case we will either have a system in the a or in the b state. In the quantum case one has a superposition of the two states. This makes it possible to perform many calculations at the same time, on all the states included in the superposition.

Entanglement

The entanglement is some sort of dependence between two states. As an example let us take a system were the sum of the spin is zero, the system consists of two particles, both having an individual spin, either up $|\uparrow\rangle$ or down $|\downarrow\rangle$. All dependence of distance between the two particles in the system will be ignored. This makes it possible to e.g. have a system with one of the particles in Lund and the other one in Paris. By measuring the state of the particle in Lund, automatically the particle located in Paris will collapse into the opposite spin.

Quantum computing in rare-earth-ion-doped crystals

Rare-earth-ion-doped crystals have some very useful properties for quantum computing. Their absorption spectrum is determined by two processes, homogeneous and inhomogeneous broadening [3], see figure 1.4. The frequency of the rare-earth-ions will be shifted by interaction with their local environment. Since the dopant ions individually will sense a different surrounding the absorption line will be inhomogeneously broadened.

The homogeneous broadening is very close to the Heisenberg limit of time-energy uncertainty of the ions. Since the ions have a certain lifetime in an energy state they will have an energy uncertainty related to that. The very narrow homogeneous broadening is because outer electrons shield the electrons used in the transitions. Therefor the electrons are not too strongly affected by the surroundings.

To make computations we need to create some sort of qubit. A qubit is the quantum computer equivalent to a classic computer bit. One of the main ideas in the experiments made in Lund is to burn a spectral hole in the absorption

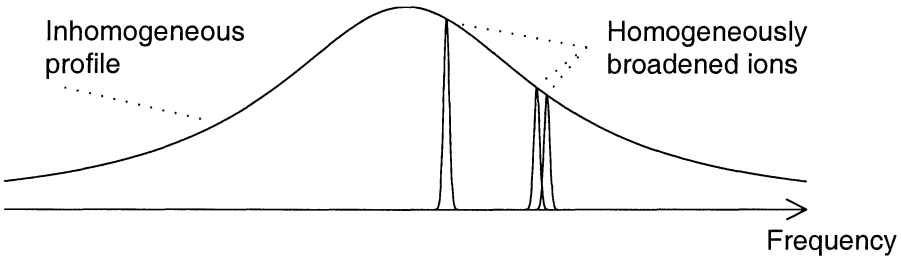

Figure 1.4: The homogeneous broadening, not much broader than the broadening given by the Heisenberg time-energy uncertainty, and the inhomogeneous, resulting from differences in the crystal environement for the dopant ions.

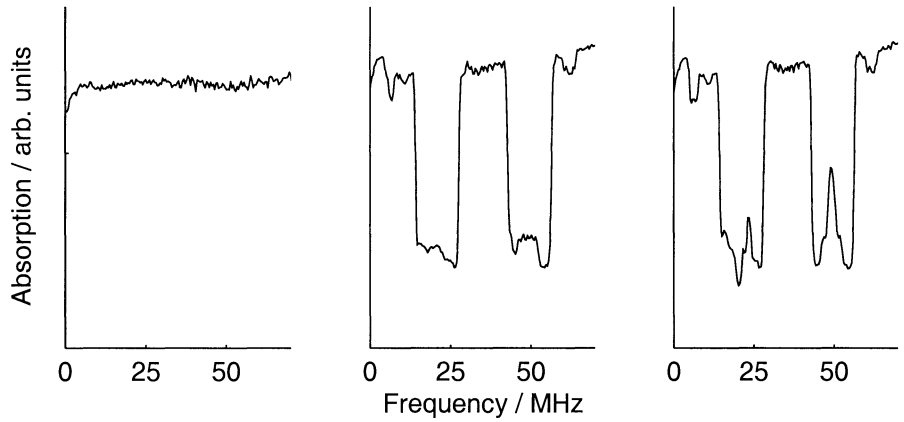

Figure 1.5: A non perturbed absorption spectrum is shown in the left figure. In the middle figure two holes are prepared for the qubits. In the right figure a qubit-one is placed in the hole center at 50 MHz.

profile. In the center of this hole we can place a group of ions absorbing at this frequency, i.e. a peak at one equivalent to $|1\rangle$, or another frequency, equivalent to $|0\rangle$. The hole is burnt by moving all the ions on a specific energy interval into an auxiliary energy level. A sharp peak is then brought back at the centre frequency of the hole, with two π-pulses, see figure 1.5

The correlation needed to make computations is an effect of dipole-dipole interaction. When ions are put in a higher energy level they will change their dipole moment. Other ions close by will be affected by this change and their energy levels will shift slightly. This effect is proportional to r^{-3}, where r is the distance between the two ions so it will only affect ions that are sufficiently close. Purification of the peak put in the hole is therefore needed. By exciting another frequency interval and then burning away, to the auxiliary level, all the ions not shifting in the hole, one gets only the ions that interact enough. The process is shown in figure 1.6.

Fundamental parts of a computer are, among others, the transistor and the controlled not, C-NOT, gate. One possible way to implement a C-NOT gate in rare-earth-ion-doped crystals has been presented in [4].

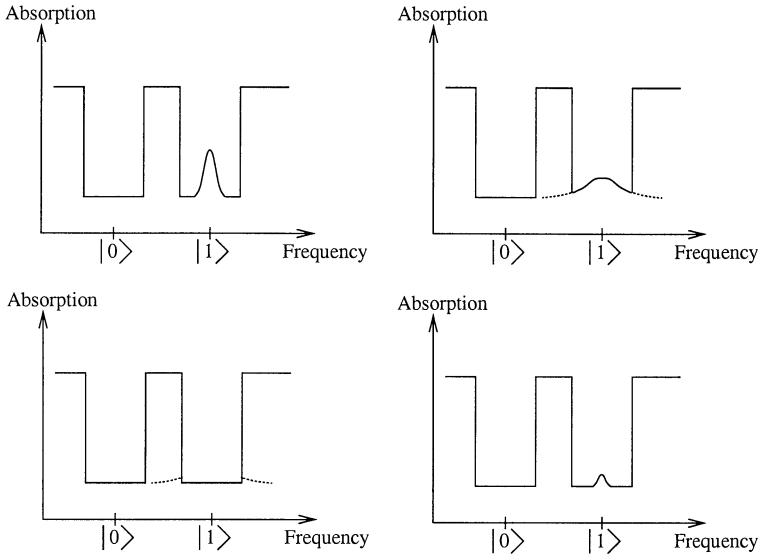

Figure 1.6: The qubit preparation and purification process. Upper left, prepare a qubit by removing all ions in a frequency interval and then returning a very narrow peak in the middle. Upper right, excite ions at a frequency interval of another interacting qubit and observe the shift. Lower left, remove the ions not shifting. Lower right, de-excite the ions excited at the interacting qubit and observe the ions shifting back into the center. All the ions left in the peak interact strongly with the ions in the other qubit and it is now possible to create correlations and entanglement between the ions in the two peaks.

With j as the control qubit and i as the target, $|0\rangle$ as the 0 state of the qubit, $|1\rangle$ as the 1 and $|e\rangle$ as the excited state.

1. π-pulse on $|0\rangle_j$ - $|e\rangle_j$
2. π-pulse on $|0\rangle_i$ - $|e\rangle_i$
3. π-pulse on $|1\rangle_i$ - $|e\rangle_i$
4. π-pulse on $|0\rangle_i$ - $|e\rangle_i$
5. π-pulse on $|0\rangle_j$ - $|e\rangle_j$

If the control qubit j was in the $|0\rangle$ state then the target will be shifted out of resonance by step 1. Step 2 to 4 will then have no effect. If j was in the $|1\rangle$ state then step 2-4 will invert the state of the i ions.

Stability requirements

For small frequency shifts of the light within the absorption profile of the crystal an Acousto Optic Modulator (AOM) is used. This way a fixed frequency laser is the light source of the experiments. The available laser is a Coherent 699 Dye laser, tuned to the preferred frequency, and it drifts a lot compared to its own bandwidth. If the laser drifts it will not have the correct frequency to hit the

peaks when we try to excite the control or the data qubits. A laser drift below 1 MHz is desired for future experiments, the goal is a maximum drift of 100 kHz.

1.2 Laser Stabilisation Techniques

The Coherent 699 Dye laser used for the experiments has an internal frequency stabilisation. Even with this stabilisation the laser drifts as seen earlier in figure 1.1. Many different techniques have been developed to solve this problem. In this master's thesis the choice has been locking onto a hyperfine level of Iodine. A small introduction to this and to another important technique will be made here below.

1.2.1 Saturation Spectroscopy and Frequency Locking to an I_2 Line

A very common stabilisation technique is used in this thesis. The 15th hyperfine component of the (v'=17, J'=61) $\rightarrow$ (v"=1, J"=62) in $^{127}I_2$ was at the "Conference Generale des Poids et Mesures" in Paris, 1983, considered a secondary standard for the length unit. The transition used for this standard is $576,29476027nm$. Since the transition structure is stable and lines can be found in a broad region of the spectrum it will be possible, with a high probability, to lock the laser frequency in a desired frequency region.

Saturation spectroscopy is used in the frequency locking scheme to obtain sub Doppler resolution. The laser light is divided into two counter propagating beams, a strong, pump, and a weak, probe. The pump beam is frequency modulated and the two beams are overlapped in a glass cell containing Iodine. After the cell the probe beam is detected with a photo diode and the signal is sent to a lock-in amplifier that detects signals at the modulation frequency of the pump beam. The probe beam transmission through the cell will be affected by the two sidebands of the pump beam, produced by the frequency modulation, when the laser is scanned over the absorption profile of Iodine. The effect will be a spectrum as in figure 1.7. The spectrum is a first order derivative of the absorption spectrum. This is an effect of the frequency modulation and will further be treated in section 2.1.3.

The big advantage of the frequency modulation compared to the amplitude modulation is that we have a very sharp edge in the middle of the hyperfine line, where the signal switches sign from positive to negative or vice versa. The frequency modulation spectrum will be the derivate of the amplitude modulation spectrum of the Lorenzian line shape. This line is perfect as an error signal. Whenever the signal becomes a bit positive the laser has drifted slightly to lower frequencies and we get an error signal telling us to compensate. For amplitude modulation we could frequency lock on the slope at one side of the Lorentzian profile of the line. The problem is that the intensity of the line will change with the laser intensity and other noise factors. An intensity change would send a false error signal to the laser control system and introduce another error to the laser stability.

The details of this system will be found in chapter 2.

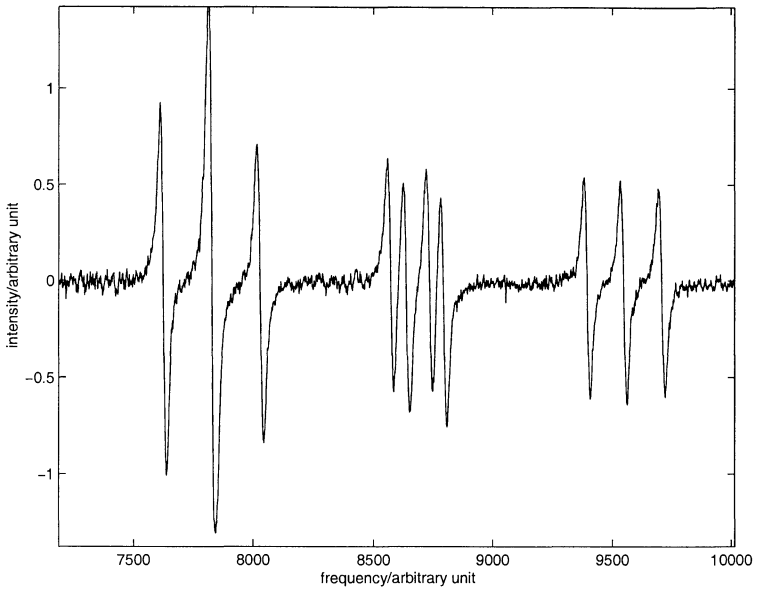

Figure 1.7: An I_2 spectrum detected with frequency modulation saturation spectroscopy. The intensity detected is the derivative of the hyperfine line profile.

1.2.2 Laser Stabilisation to Spectral Hole Burning

Laser Stabilisation to Spectral Hole Burning was first presented in [5]. Here a narrow hole was burnt in the absorption profile of $CaF_2 : Tm^{3+}$ in a similar way as was done in figure 1.5. This hole was detected with the laser that is to be stabilised. To detect the hole without continuing to burn it (which would result in that the hole moves if the detection was at one side of the hole) a very low laser intensity was used. Electro-optic modulators were used to modulate the frequency and the very weak signal was detected using lock-in technique. As in this thesis the light was frequency modulated to produce a good feed-back signal.

To stabilise the laser system to a spectral hole in a crystal is proposed to be the next step in laser stabilisation in the photon echo group at Lund Institute of Technology. The use of Iodine as a reference is problematic when the Iodine lines are far from the desired frequency region. Since the absorption profiles of the crystals that the group works with can be used as reference media there will never be that kind of problems. Part of the equipment needed already exists in the laboratory which makes it less expensive to build.

Chapter 2

Stabilisation

2.1 Detection Techniques

To lock a laser to a hyperfine level in I_2, a better resolution than the Doppler broadened profile is needed. In this section there is a description of the technique used and some comparasion with related methods.

2.1.1 Modulation

Modulation techniques are used to find very small signals in a noisy background. The basic principle is to move the detection to higher frequencies were the noise is lower and to use filters to retrieve the signal. Amplitude Modulation (AM), Frequency Modulation (FM) and fast scan integration are some examples of common modulation techniques.

2.1.2 Amplitude Modulation

Amplitude modulation is the easiest method. By chopping the laser beam before it enters the sample and detecting with a lock-in amplifier the signal is easily recorded. This method, however, is not suitable for stabilising the laser. If we use the side of the absorption peak (a Lorenzian function) as our error signal we will get a laser drift every time the detection efficiency or the laser power changes. In figure 2.1 we can see a Lorenzian function. The left flank of the function can be used as reference. The desired frequency will be the one at half the maximum amplitude of the Lorenz profile. If the frequency increases, the output is an error signal proportional to the increase of amplitude from the Lorenzian. The regulator compensates by adjusting the frequency until the error signal vanishes. This works well as long as the system detects the signal strength of the Lorenzian profile. If the laser increases its amplitude there will be a lower frequency corresponding to the zero-error signal. This will cause the laser to actively regulate to a lower, non-wanted frequency. This problem can however be avoided by using frequency modulation.

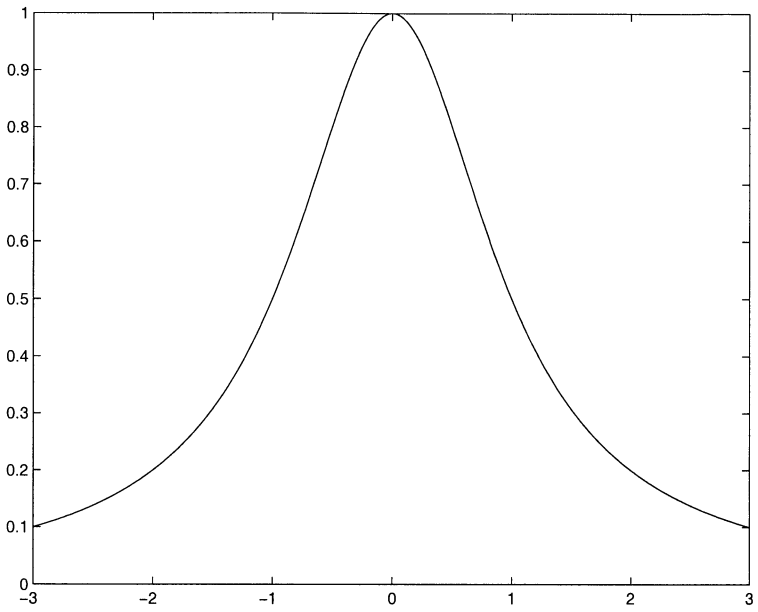

Figure 2.1: Lorenzian profile.

2.1.3 Frequency Modulation

Frequency modulation (FM) is a well-developed technique used since the late seventies [6]. When using diode laser the laser frequency can easily be modulated by adding a sinusoidal voltage on the frequency control of the laser driver. In experiments of the quantum computer research in the photon echo group in Lund, no extra or added noise was wanted since the lasers bandwidth was to be kept low. It is not easy to modulate the Coherent 699 Dye laser used here without significantly modifying the laser design. An external Acousto Optic Modulator (AOM) was therefore used to modulate the light. By adding a sinusoidal signal to the frequency control on the AOM, frequency-modulated laser light was obtained.

The Acousto Optic Modulator

An Acousto Optic Modulator (AOM) works as an adjustable grating. The light traverses across a perpendicular acoustic standing wave which acts as the grating. The grating slits are created from the differences caused by the nodes and anti nodes of the acoustic wave. A wave diffracted in the first order will absorb a momentum of the phonon in the standing wave. By modulating the frequency of the AOMs standing wave an added frequency of $2\pi(\nu_{AOM} + \beta sin(2\pi\nu_{FM}))$ is the result. β is the amplitude of the added frequency oscillation, the so called modulation depth.

Mathematical Survey of the Frequency Modulation

A brief introduction to frequency modulation will be given. For deeper knowledge reference is made to [7, 8].

Consider a non modulated wave with optical carrier frequency ν_c

$$E_1 = E_0 exp[\imath 2\pi\nu_c t]$$

Adding a frequency modulation of the type $2\pi(\nu_{AOM}+\beta sin 2\pi\nu_{FM})$ in an AOM will produce an electric field leaving the AOM of

$$E_2 = E_0 exp[\imath 2\pi(\nu_c + \nu_{AOM} + \beta sin 2\pi\nu_{FM})t] \tag{2.1}$$

which can be expressed as an expansion in Bessel functions [9]

$$E_2 = E_0 \sum_{n=-\infty}^{\infty} J_n(\beta) exp[\imath 2\pi(\nu_c + \nu_{AOM} + n\nu_{FM})t] \tag{2.2}$$

In the frequency spectrum this will be a centre frequency with pairs of sidebands separated ν_{FM}. The relation $J_{-n}(\beta) = (-1)^n J_n(\beta)$ will make the sidebands of odd ns π radians out of phase to one another.

The light will then interact with absorbative material and be affected in amplitude and phase. As an operator it can be written $T(\nu) = exp[-\alpha(\nu) - \imath\phi(\nu)]$. α is here the absorption at the frequency ν and ϕ is the corresponding phase change. The electric field after the sample is then

$$E_3 = E_0 \sum_{n=-\infty}^{\infty} T(\nu_c+\nu_{AOM}+n\nu_{FM}) J_n(\beta) exp[\imath 2\pi(\nu_c+\nu_{AOM}+n\nu_{FM})t] \tag{2.3}$$

β is the amplitude of the modulation. If β is low then approximations of $J_0(\beta) \approx 1$ and $J_{\pm 1}(\beta) \approx \pm\beta/2$ can be made. All the other terms will be negligible. E_3 will then simplify to

$$\begin{aligned} E_3 \approx\ & E_0\{T(\nu_c+\nu_{AOM}) exp[\imath 2\pi(\nu_c+\nu_{AOM})t] && (2.4)\\ & +\frac{1}{2}T(\nu_c+\nu_{AOM}+\nu_{FM})(\beta) exp[\imath 2\pi(\nu_c+\nu_{AOM}+\nu_{FM})t] && (2.5)\\ & -\frac{1}{2}T(\nu_c+\nu_{AOM}-\nu_{FM})(\beta) exp[\imath 2\pi(\nu_c+\nu_{AOM}-\nu_{FM})t]\}. && (2.6) \end{aligned}$$

If detecting the intensity on a photo detector $I(t) = c\varepsilon_0 EE^*/2$ is recorded and by dropping terms of order greater than β^2 ($\beta << 1$) the approximation is reduced to

$$\begin{aligned} I(t) =\ & \frac{c\varepsilon_0}{2} E_0^2 exp(-2\alpha_0)\{1 + [exp(-\alpha_0+\alpha_1)cos(\phi_1-\phi_0)\\ & -exp(-\alpha_0+\alpha_{-1})cos(\phi_0-\phi_{-1})]\beta cos(2\pi\nu_{FM}t)\\ & +[exp(-\alpha_0+\alpha_1)sin(\phi_1-\phi_0)\\ & -exp(\alpha_0+\alpha_{-1})sin(\phi_0-\phi_{-1})]\beta sin(2\pi\nu_{FM}t)\} \end{aligned}$$

which is achieved with $\alpha_n \equiv \alpha(\nu_c+n\nu_{FM})$, $\phi_n \equiv \phi(\nu_c+n\nu_{FM})$ and $n = -1, 0, 1$. By supposing that the differences between the absorption and dispersion in the carrier and the sidebands are small, i.e. $\mid \alpha_0 - \alpha_{\pm 1} \mid << 1$, and $\mid \phi_0 - \phi_{\pm 1} \mid << 1$, we get

$$\begin{aligned} I(t) =\ & \frac{c\varepsilon_0}{2} E_0^2 exp(-2\alpha_0)[1 + (\alpha_{-1}-\alpha_1)\beta cos(2\pi\nu_{FM}t) && (2.7)\\ & +(\phi_1+\phi_{-1}-2\phi_0)\beta sin(2\pi\nu_{FM}t)] && (2.8) \end{aligned}$$

The cosine term will then give the ratio of absorption difference between the upper and the lower sideband. The sine term will give the ratio between the phase shift between the different sidebands compared to the main frequency. If $\delta\nu >> \nu_{FM}$, i.e. the width of the absorption feature is much larger than the modulation frequency, the cosine term will be proportional to the derivative of the absorption line at frequency $\nu_c + \nu_{AOM}$.

2.1.4 The Lock-in Technique

The Lock-in amplifier works on the principle of a very narrow adjustable filter combined with a high amplification [10]. Very weak signals drowned in noise, 1000 times stronger than the signal can be detected. The signal, typically of the strength of tens of nV can give an output of 10 V.

The experimental output signal needs to be modulated at one, fixed, frequency. This frequency must be known by the lock-in amplifier. The modulation frequency should normally be in the upper bound of the lock-in amplifiers range (see section 2.6) to reduce the $1/f$ noise. Typically the bandpass has a Q of 106.

The incoming reference signal is detected in the Phase-Lock loop (PLL). The PLL output is a signal of the type $cos(2\pi\nu_{ref}t + \Phi)$ where ν_{ref} is the reference frequency and Φ is an adjustable phase. The input signal from the experiment is multiplied with the PLL output in a Phase-Sensitive Detector (PSD) which will give the output

$$cos(2\pi\nu_{ref}t + \Phi)cos(2\pi\nu_{sig}t) = \frac{1}{2}cos[2\pi(\nu_{ref} + \nu_{sig})t + \Phi] + \\ + \frac{1}{2}cos[2\pi(\nu_{ref} - \nu_{sig})t + \Phi].$$

ν_{sig} is the frequency from the signal.

After the multiplier there is a low pass filter that attenuates the higher frequency term. Only the differential DC term, proportional to the signal, is left. The signal is maximised by tuning the phase Φ.

2.2 Doppler broadening

Doppler broadening or Doppler shift is a frequency change of waves emitted or absorbed by moving objects. An everyday experience of the Doppler effect is the change of the sound from the high-speed train passing by. When the train is closing in, the sound frequency will be high and when it is going away it will be low.

In this section the Doppler shift of electro-magnetic (light) waves will be discussed. Since the light does not need a media to travel the only speed of interest is the relative speed of the emitter towards the listener. In the case of sound waves, the listener and the emitter are moving relative to the media transporting the waves and a different kind of calculation is needed, see [11].

The positive relative speed is defined as when the emitter is approaching the observer who is always supposed to stand still.

Imagine the emitter of a frequency f_s moving with the relative velocity v_s. The wavelength, i.e. the distance between two crests, seen by the observer is

searched. The time between the crests in the emitting reference is $T_s = 1/f_s$. The emitter will have moved a distance $d = v_s T_s$ between two crests. The first crest will be a distance of cT_s away from the original location when the second crest is emitted. The wavelength seen by the observer will then be $\lambda_o = (c - v_s)T_s$ and will therefore have the frequency

$$f_o = \frac{c}{\lambda_o} = \frac{c}{(c - v_o)T_s}. \tag{2.9}$$

However this equation is not relativistically correct to equate T_s, the time in the emitter reference, with T_o, in the observers reference. To correct for relativistic effect a Lorentz transformation must be made.

$$T_s = \frac{T_o}{\sqrt{1 - v_s^2/c^2}} \tag{2.10}$$

Combining the result of equation 2.9 and 2.10 produces, after some simplification

$$f_o = \frac{\sqrt{c + v_s}}{\sqrt{c - v_s}} f_s$$

This shows the statement at the beginning of this section that an object moving towards the listener will be observed with a higher frequency than emitted and vice versa.

As in most cases the relative speed is much lower than the speed of light and the formula can be simplified to

$$\frac{\Delta f}{f} = \frac{v_s}{c}.$$

The atoms in a gas move around randomly at different speeds. Identical atoms will absorb and emit light at a specific frequency. Since they move randomly the observed frequency will change and the total absorption line will become Doppler broadened. Atoms moving towards a light source will absorb radiation at a higher frequency than those moving away. Since the atoms are affected individually the broadening is inhomogeneous. The broadening is often too large to resolve closely lying absorption frequencies like hyperfine structure. In such cases other, more sophisticated, detection techniques will be needed to obtain the required resolution.

More information about Doppler shifts can be found in almost any book on general or atomic physics, such as [11, 12].

2.3 Hyperfine structure

A very brief introduction on atomic physics, to make the reader familiar with the term hyperfine structure, will follow. Atoms have different quantisised energy levels. For hydrogen the energies of the principal energy levels, E_n, is given by

$$E_n = -\frac{13.60eV}{n^2}$$

where n is called the principal quantum number.

An electron going around the nucleus will have an orbital angular momentum called **L**. The electron also possesses an internal angular momentum, comparable to the rotation of earth around its own axis. The later one is called the electron spin. The magnitudes of **L** and **S** are

$$| \mathbf{L} | = \hbar\sqrt{l(l+1)}, (l = 0, 1, 2, ..., n-1)$$
$$| \mathbf{S} | = \hbar\sqrt{s(s+1)}, (s = \pm\frac{1}{2})$$

An energy shift will be produced by the interaction between the spin and the orbital angular momentum. A structure is made by the shift, called the finestructure or L-S coupling. The shift will have the form

$$\Delta E_{LS} = \frac{A}{\hbar^2}\mathbf{S} \cdot \mathbf{L}.$$

A is called the finestructure constant. To calculate ΔE_{LS} there is need to rewrite $\mathbf{S} \cdot \mathbf{L}$. By taking the square of **J**, the sum of **S** and **L**, the scalar product will be solvable. Note also that the magnitude, and therefore the squares of **L**, **S** and **J**, are known.

$$\mathbf{J} = \mathbf{S} + \mathbf{L}$$

$$\mathbf{J}^2 = (\mathbf{S} + \mathbf{L})^2 = \mathbf{S}^2 + \mathbf{L}^2 + 2\mathbf{S} \cdot \mathbf{L}$$
$$\mathbf{S} \cdot \mathbf{L} = \frac{1}{2}(\mathbf{J}^2 - \mathbf{L}^2 - \mathbf{S}^2) = \frac{\hbar^2}{2}[j(j+1) - l(l+1) - s(s+1)]$$

Like electrons the nuclei have an internal angular momentum. This angular momentum, called the nuclear spin, **I**, interacts with the electrons and gives an energy splitting called hyperfine structure. Like the other momenta above the magnitude of **I** is

$$| \mathbf{I} | = \hbar\sqrt{I(I+1)}$$

Every neutron and proton holds a spin of $\pm\frac{1}{2}$. The total value for the nucleus is the sum of the individual protons and neutrons. For stable atoms this value will vary between 0 and 15/2. The total angular momentum for the atom is

$$\mathbf{F} = \mathbf{J} + \mathbf{I}.$$

With the same method as above, and with a hyperfine structure constant called a the hyperfine splitting in energy becomes

$$\Delta E_{hfs} = \frac{a}{\hbar^2}\mathbf{F} \cdot \mathbf{J} = \frac{a}{2}[F(F+1) - j(j+1) - I(I+1)]$$

The hyperfine structure gives a very small energy shift. This shift is normally much smaller than the Doppler broadening discussed in section 2.2.

To read more about the hyperfine structure see for example [13] or any other book on basic atomic physics.

2.4 The I_2 Molecule

A notation close to that of atoms is used for molecules. Iodine is described by

$$^{\Sigma}\Lambda_{\Omega} \tag{2.11}$$

In a symmetric molecule like Iodine only the projection of the total angular momentum **L** on the symmetry axis is constant of motion. The projection is characterized by the quantum number M_L,

$$M_L = L, L-1, ... -L.$$

The energy does not change by the exchange $M_L \rightarrow -M_L$ since the inter-nuclear field is of electric and not magnetic nature. Λ in equation 2.11 is then designated by the absolute value of M_L

$$\Lambda = \mid M_L \mid .$$

The different states are given the same way as for the **L** values for atoms but here written with Greek letters

$$\begin{array}{cccccc} \Lambda & = & 0 & 1 & 2 & 3 \\ & & \Sigma & \Pi & \Lambda & \Phi. \end{array}$$

The total spin quantum number has $2S+1$ different projections on the symmetry axis of the molecule. As for atoms this is written on the place of Σ in equation 2.11.

Also the projection of **J** exists for the molecules. This is called Ω and is as for atoms obtained from Λ and Σ

$$\Omega = \Lambda + \Sigma, \Lambda + \Sigma - 1, ... \mid \Lambda - \Sigma \mid$$

Iodine is a homo-nuclear molecule, containing two equal atoms. Because of the symmetry of the molecule the parity of the function can be classified as g (German 'gerade') for even and as u (German 'ungerade') for odd. This parity is written next to Ω in equation 2.11 giving, for u

$$^{\Sigma}\Lambda_{\Omega u}$$

Since Iodine is a particle with half spin it obeys Fermi-Dirac statistic and therefore its total wave function is anti-symmetric [14]. Two nuclei cannot have all their quantum numbers equal according to the Pauli's exclusion principle.

The projection of the Iodine atoms nuclear spin **I** of 5/2 along the **J**-axis in the Iodine molecule gives $2 * 5/2 + 1 = 6$ different energy level. As two atoms are present there should then be 36 hyperfine lines hid in every Doppler line of Iodine. As a whole molecule built up by fermions, Iodine must be anti-symmetric [15] which will make some of those levels forbidden. As a result there will be 15 or 21 lines [16] in every broadened profile depending on whether **J** is odd or even at the basic energy level.

2.5 Saturation Spectroscopy of Iodine

Saturation spectroscopy has for a long time been a simple and efficient method for accomplishing sub-Doppler measurements. There are numerous books and articles written on the topic, among them [3, 12, 17, 18, 19, 20, 21, 22].

A brief introduction to the method will be presented. Knowledge about the atomic susceptibility is first needed. The reason is that nonlinear atomic response to saturation, which is required for the sub-Doppler resolution, can be conveniently described in terms of the susceptibility.

2.5.1 Atomic Susceptibility

Electric Susceptibility

While working with linear and isotropic media there is a linear relation between the applied electric field, $\mathbf{E}$ and the polarisation $\mathbf{P}$ in the media.

$$\mathbf{P} = \epsilon_0 \chi_e \mathbf{E}$$

Here χ_e is called the electric susceptibility.

In a dielectric media this will yield an electric displacement $\mathbf{D}$ of

$$\begin{aligned} \mathbf{D} &= \epsilon_0 \mathbf{E} + \mathbf{P} \\ &= \epsilon_0 (1 + \chi_e) \mathbf{E} \\ &= \epsilon_0 \epsilon_r \mathbf{E} \\ &= \epsilon \mathbf{E} \end{aligned}$$

ϵ_r is called the relative permittivity or the dielectric constant and is a dimensionless constant (in air it is $1,0059$). ϵ is the absolute permittivity measured in farads per meter (F/M). The dimension is inherited from the permittivity of free space, ϵ_0.

A media is called homogeneous if ϵ_r is independent of position. It is isotropic if it is independent of direction. It is called linear if it does not have any nonlinear effects.

For deeper knowledge of electric susceptibility se [3, 23, 24].

Atomic Susceptibility

The macroscopic polarization p in one dimension will obey the equation of motion and decay because of the oscillation amplitude decay (γ) and the random de-phasing T_2, see further [3].

$$\frac{d^2 p_x(t)}{dt^2} + (\gamma + 1/T_2)\frac{dp_x(t)}{dt} + \omega_a^2 p_x = (Ne^2/m)\mathbf{E}_x(t) \tag{2.12}$$

where ω_a is the resonance frequency of the atom, N is the number of atoms involved and $\mathbf{E}$ is the driving electric field that has the form

$$\mathbf{E}_x = Re[E_x e^{\imath\omega t}] = \frac{1}{2}[E_x e^{\imath\omega t} + c.c.]$$

The phase is set to zero for simplicity.

The induced polarization p_x of the system will be of the same form

$$p_x = Re[P_x e^{\imath\omega t}] = \frac{1}{2}[P_x e^{\imath\omega t} + c.c.]$$

To simplify the writing it will only be written

$$\mathbf{E}_x = E_x e^{\imath\omega t}$$

further on, taking the real part being understood.

By putting this into the equation of motion (2.12) and carrying out the derivatives it becomes

$$[-\omega^2 + \imath\omega(\gamma + 2/T_2) + \omega_a^2]P_x = \frac{Ne^2}{m}E_x$$

which gives the definition of atomic susceptibility[1] in the same way as the electrical in section 2.5.1.

$$\chi_{at} = \frac{P_{at}(\omega)}{\epsilon E(\omega)} \tag{2.13}$$

$$= \frac{Ne^2}{m\epsilon}\frac{1}{\omega_a^2 - \omega^2 + \imath\omega\Delta\omega_a} \tag{2.14}$$

with the atomic linewidth (FWHM) of the atomic resonance, see [3]

$$\Delta\omega_a \equiv \gamma + 2/T_2.$$

In the resonance region, i.e. $\omega \approx \omega_a$ the equation (2.13) can be rewritten as

$$\chi_{at}(\omega) = \frac{-\imath Ne^2}{m\omega_a\epsilon\Delta\omega_a}\frac{1}{1 + 2\imath(\omega - \omega_a)/\Delta\omega_a}.$$

The equation is then a typical complex Lorentzian. This is acompliched with the approximation

$$\omega^2 - \omega_a^2 = (\omega + \omega_a)(\omega - \omega_a) \approx 2\omega_a(\omega - \omega_a) \approx 2\omega(\omega - \omega_a),$$

which gives

$$\frac{1}{\omega_a^2 - \omega^2 + \imath\omega\Delta\omega_a} \approx \frac{1}{2\omega_a(\omega_a - \omega) + \imath\omega_a\Delta\omega_a}.$$

This quality gives a narrow resonance peak. As long as we keep within some orders of $\Delta\omega_a$ it will give a big response, outside of this region the signal quickly decreases.

Introducing some new definitions makes it possible to rewrite the equation in a more readable way.

$$\Delta x \equiv 2\frac{\omega - \omega_a}{\Delta_{\omega_a}} \tag{2.15}$$

$$\chi_0'' \equiv \frac{Ne^2}{m\omega_a\epsilon\Delta\omega_a} \tag{2.16}$$

[1] definition used by Siegman [3]

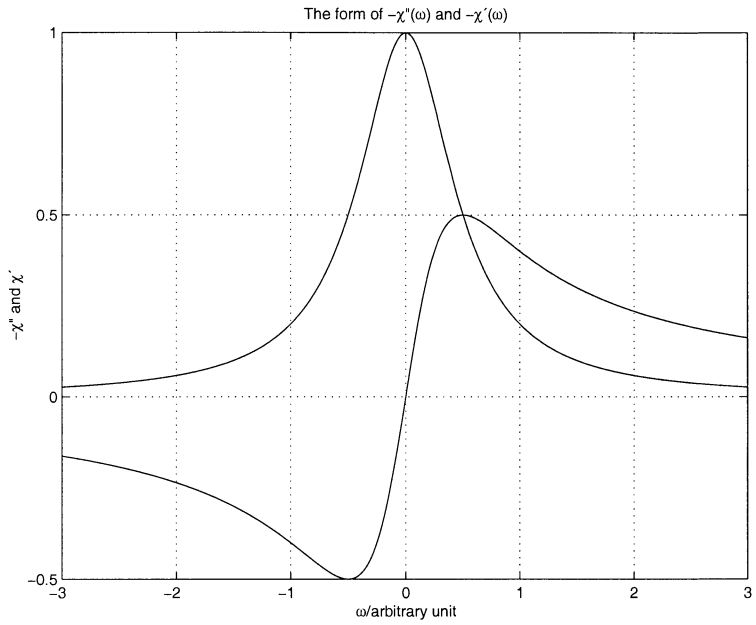

Figure 2.2: The real and imaginary parts of the complex Lorentzian lineshape. As seen in equation 2.17 χ' is an odd function and χ'' is even.

Equation 2.15, 2.16 and separating the real and imaginary parts of $\chi_{at}(\omega)$ gives

$$\chi_{at}(\omega) \equiv \chi'(\omega) + \imath\chi''(\omega) = -\chi_0'' \left[\frac{\Delta x}{1+\Delta x^2} + \imath \frac{1}{1+\Delta x^2} \right]. \tag{2.17}$$

$\chi'(\omega)$ and $\chi''(\omega)$ are called the real and imaginary parts of the function, plotted in figure 2.2. The imaginary part $\chi''(\omega)$ is the one causing absorption or amplification and the real part $\chi'(\omega)$ causes phase shift or dispersion. This can be compared to the effects of complex index of refraction [25]. Detection of $\chi''(\omega)$ is discussed in section 2.5.3. This is also the base for the frequency stabilisation scheme in this thesis. To make the discussion complete detection of $\chi'(\omega)$ is presented in section 2.5.4.

2.5.2 Hole Burning

Burning a hole in an absorption profile means that atoms of a chosen energy state are excited to another. If all atoms are moved like this the media will no longer have any absorption at the chosen frequency and therefore a hole in the absorption profile is created.

A more theoretical way of describing the hole burning effect is that the imaginary part $\chi''(\omega)$ of the susceptibility is changed. In this section the expression 2.17 will be generalised to treat inhomogeneous profiles. Above, in section 2.5.1 the discussion has only concerned homogeneous broadening. The adaption is quite straightforward and doesn't require too many changes.

In an inhomogeneously broadened material all atoms will react in the same way in their own inertial system. The big difference is that their resonance

frequencies will all be individual from an external point of view. This can for example be someone detecting the resonance frequency of a gas. All the atoms will in rest have the same resonance frequency, but viewed with the Doppler shift, they will have a distribution of their resonance frequencies. The distribution is here called $g(\omega_a)$, were ω_a is the resonance frequency for atoms in a $d\omega_a$ interval. The distribution will be normalised as

$$\int_{-\infty}^{\infty} g(\omega_a)d\omega_a = 1.$$

If the total number of atoms is N, the amount in a certain frequency interval at ω_a, $dN(\omega_a)$, can then be written

$$dN(\omega_a) = Ng(\omega_a)d\omega_a.$$

A steady state atomic saturation is now introduced (see further [3]). The saturation intensity I_{sat} is also defined as follows. The intensity that reduces the population difference between two levels to half of its original value is called the saturation intensity I_{sat}. The saturation factor can then be introduced as the factor between the population difference at intensity I compared to the original population difference.

$$S(\omega_a) \equiv \frac{population\,difference}{original\,population\,difference} = \frac{1}{1 + I/I_{sat}\sigma}$$

were σ is the cross section for a transition of Lorenzian frequency distribution affected by the frequency ω_1

$$\sigma = \frac{1}{1 + [2(\omega_1 - \omega_a)/\Delta\omega_a]^2}.$$

the homogeneous susceptibility in equation 2.17 can now be generalised to the total susceptibility $\chi(\omega)$.

$$\chi(\omega) = N\int_{-\infty}^{\infty} g(\omega_a)S(\omega_1;\omega_a)\chi_{at}(\omega;\omega_a)d\omega_a$$

The integral is not a very nice one to solve and approximations are needed. By calculating the change in susceptibility, $\delta\chi(\omega)$ caused by saturation intensity I, many difficulties are avoided. The unperturbed susceptibility is called $\chi_0(\omega)$.

$$\begin{aligned}
\delta\chi(\omega) &\equiv \chi(\omega) - \chi_0(\omega) = \\
&= N\int_{-\infty}^{\infty} g(\omega_a)[S(\omega_1;\omega_a) - 1]\chi_{at}(\omega;\omega_a)d\omega_a \\
&= \dots \\
&= N\chi_0''\int_{-\infty}^{\infty} g(\omega_a) \times \left[\frac{I/I_{sat}}{1 + I/I_{sat} + [2(\omega - \omega_a)/\Delta\omega_a]^2}\right] \times \\
&\quad \times \left[\frac{1}{1 + 2j(\omega - \omega_a)/\Delta\omega_a}\right] d\omega_a
\end{aligned}$$

In the realistic case where the inhomogeneous broadening $g(\omega_a)$ is very large this term can be moved outside the integral. The integral can then be solved with residue theory and will after some steps (see [3]) become:

$$\delta\chi(\omega) = N\chi_0''\pi \times \frac{\sqrt{1 + I/I_{sat}} - 1}{\sqrt{1 + I/I_{sat}}} \times \frac{1}{1 + 2j(\omega - \omega_1)/\Delta\omega_{hole}}. \qquad (2.18)$$

Here $\Delta\omega_{hole} \equiv (1+\sqrt{1+p})\Delta\omega_a$ is the linewidth of the burnt hole. For very weak or strong saturation the following approximations can be made:

$$\Delta\omega_{hole} \equiv (1+\sqrt{1+p})\Delta\omega_a \approx \begin{cases} 2\Delta\omega_a & I << I_{sat} \\ \sqrt{I/I_{sat}}\Delta\omega_a & I >> I_{sat}. \end{cases}$$

The saturation depth, i.e. the amount of population difference removed, can also be approximated in the same cases:

$$\frac{\sqrt{1+I/I_{sat}}-1}{\sqrt{1+I/I_{sat}}} \approx \begin{cases} I/(2I_{sat}) & I << I_{sat} \\ 1 & I >> I_{sat}. \end{cases}$$

The conclusion is that by irradiating a sample with light of a certain frequency a hole in the absorption profile will be burnt. The hole will for weak saturation have a linewidth of twice the atomic linewidth. The depth of the hole will increase linearly with the intensity. At strong saturation the hole will be burnt to the bottom and the width, and therefore also the area of the hole continues to increase with intensity. An easy way to detect the hole is to scan the frequency of another laser beam over the hole. The intensity must be weak enough not to burn any holes. The transmission through the sample will then increase when passing over the hole. This will be discussed in section 2.5.3 below.

2.5.3 Absorbative Saturation Spectroscopy

Saturation spectroscopy can be made in many ways. The main idea is that sub-Doppler resolution should be achieved. A hole is burnt in the absorption profile by a strong laser beam, called the pump, and is then detected by a weaker beam, called the probe. The beams are traversing the sample in opposite directions, making it possible to detect only the atoms with zero speed in the beam directions. Since the detected atoms speed is zero, a non-Doppler broadened line profile is detected.

A Typical Experiment

In a typical experiment, the beam from a tuneable laser is divided into two , the pump and the probe beam. Those enter the cell, containing the gas of interest, from opposite directions. After the cell the probe is detected and analysed, see figure 2.3. By tuning the laser over the Doppler profile a spectra of the Doppler profile with a dip at the centre will be detected, as in figure 2.4.

Detection of Different Velocity Groups

When the laser is scanned over, e.g. the hyperfine structure in Iodine, the pump will burn a hole in the absorption spectra after having interacted with all the atoms absorbing at the laser frequency. As the laser is scanned the hole will pass from one hyperfine level to another, since they are widely separated in frequency (tens to hundreds of MHz).

The atoms at a specific hyperfine level will have a velocity distribution like in figure 2.5. When the laser frequency is slightly higher than the hyperfine splitting of an atom in rest, the pump beam will burn a hole on the atoms in the velocity group moving away from it. Those atoms will be Doppler shifted

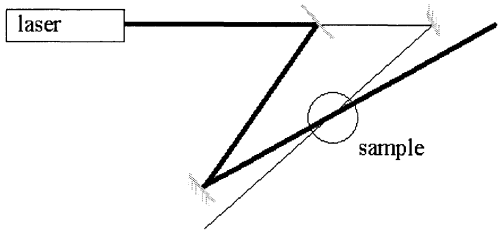

Figure 2.3: The basic saturation spectroscopy experimental set-up. The laser beam is split into two beams, the pump, which is thick and the probe, which is thin. The beams will then overlap in the sample. The overlapping angle should be kept small. After the sample the probe is detected.

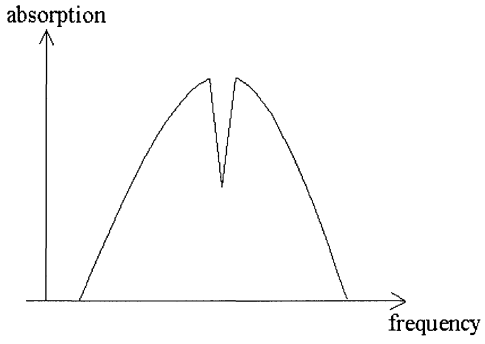

Figure 2.4: The detected absorption spectra when scanning the laser over the Doppler profile in saturation spectroscopy. The depth and width of the dip in the middle are exaggerated.

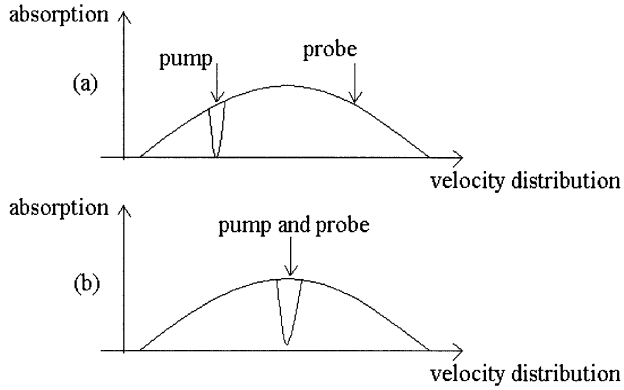

Figure 2.5:

to a higher frequency. The probe will at the same time detect at the velocity group moving in the opposite direction as in figure 2.5 (a). When the laser is tuned to a lower frequency both the pump and the probe will 'talk' to the same atoms. The probe will now detect a diminution of the absorption. The result of this detection technique produces a spectra like in figure 2.4 with a dip at every hyperfine line-centre.

Detecting With Lock-in Technique

Using lock-in technique as discussed in section 2.1.4 makes it possible to detect small changes in absorption with a high precision. The inhomogeneous broadening will not be seen at all. The only thing coming out of the lock-in amplifier will be a peak (positive or negative, depending on the phase) at every hyperfine level.

2.5.4 Refractive Index Saturation Spectroscopy

To detect the dispersion part, see section 2.5.1, in saturation spectroscopy a different experiment must be made. This was not an experimental part of this thesis but will be discussed to make a more complete picture of saturation spectroscopy. The first experiment of this kind was performed by Couillaud and Ducasse and is presented in [22]. The experimental set-up in [22] is almost the same as for absorptive saturation spectroscopy (figure 2.3). The probe beam travels in nearly opposite direction compared to the pump. Due to changes in susceptibility, caused by the pump beam, the media will work as a lens for the probe beam. The result will be a small deviation of the probe direction.

In an experiment as in section 2.5.3 the detector size is large compared to the deviation of the probe beam. The result is that the hole intensity will always be detected, independent of the deviation effect. Therefore a pure absorption saturation spectra is the result. If this was not the case the refractive index effect would easily be detected just by turning the phase of the lock-in amplifier

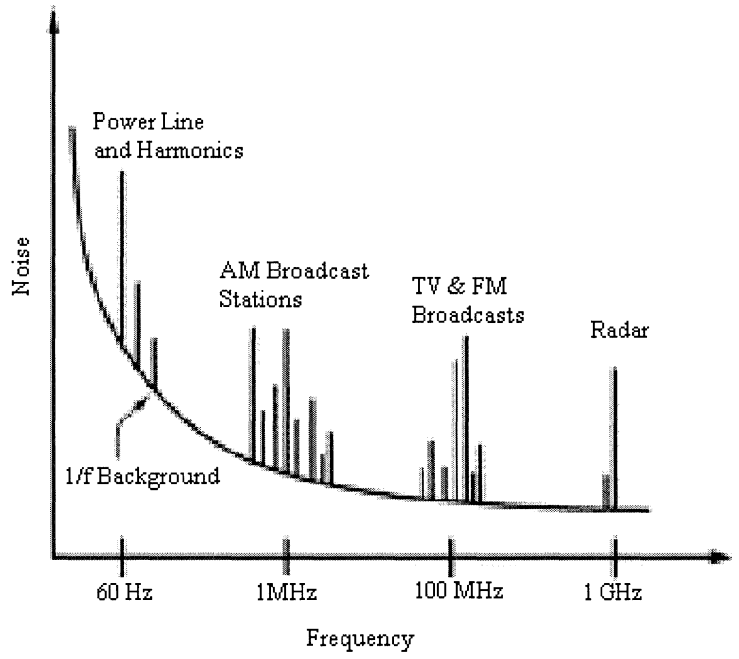

Figure 2.6: A typical noise spectra in a laboratory environment. Figure from [10].

90° from the absorbative saturation spectroscopy phase, as those effects are exactly out of phase according to the calculations made in section 2.1.3.

To detect the dispersion saturation the experiment must be changed. A probe that does not hit the detector at the centre will, when deviated, change the intensity recorded on the detector. Since the deviation is small, a large distance is needed between the experiment and the detector. For experimental data and set-up, reference is made to [22] for amplitude-modulated measurements and to [6] for frequency-modulated measurements.

2.6 Noise

Noise is always present. It can be reduced in many ways by changing positions of cables and detectors. Screening high frequency equipment is also an important task. Even with all electric gadgets turned off there will be a background noise. This noise is called Johnson noise or white noise. This noise originates from fluctuation of electron density in resistors at finite temperature [10]. In figure 2.6 this Johnson noise, that has an intensity proportional to $1/f$, where f is the detection frequency, is plotted. Also some other strong, man made, noise sources are plotted.

As clearly seen in figure 2.6 a detection at higher frequency is preferred. This can be accomplished by using i.e. the lock-in technique (see section 2.1.4). In an article by N.H. Tran and co-workers [21], the change in signal to noise (S/N) versus detection frequency is evaluated. Their conclusion is that the S/N

increases linearly with the frequency. In this article the modulation frequency is always higher than the bandwidth of the laser. This is not the case with the equipment used in this thesis. However, a combination of the conclusions in [10] and [21] is that detection at a high frequency will efficiently reduce noise.

2.7 The Stabilisation of the 699 Coherent Ring Dye Laser

2.7.1 Introduction

The main task of this thesis has been to stabilise a 699 Coherent Dye Laser. The sections before this one have been an introduction to the theory used for the stabilisation.

The main idea is to use the hyperfine structure of Iodine, a stable structure, as reference for the laser wavelength. The Iodine hyperfine levels are widely spread and the chances of having lines in the preferred frequency regions are good.

The main inspiration for this project is taken from work done by Kristin Bjornsen at Colorado State University, USA [26]. This reference gives a good description of the idea and set-up of the stabilisation.

2.7.2 Internal Laser Stabilisation

The Coherent 699-21 Dye Laser is equipped with an internal stabilisation system. This system is supposed to keep the laser at a chosen frequency with a low (1MHz) bandwidth. For many applications this system is not stable enough, as discussed in section 1.1. The laser stability was measured by Tomas Christiansson [1] and the result was presented in figure 1.1.

The internal stabilisation system [27] consists of a thermally stabilised Fabry-Perot interferometer. A small portion of the output power is directed to the Fabry-Perot interferometer using a beamsplitter right after the output mirror in the laser. The beamsplitter produces two reflections, one from each surface. One reflection is used as a laser power reference and is detected by a photo diode. The other beam goes into the interferometer and thus a combined frequency-power information signal is obtained. Since information about the power of the laser is already known, a pure frequency reference signal can be produced from the signal from the Fabry-Perot. This signal is used as a frequency reference for the stabilisation feedback system. A fringe pattern is produced and the laser frequency is locked at a midpoint at one fringe. To scan the laser the length of the Fabry-Perot is changed. An error signal will be produced since the position is no longer at the middle of the fringe. The laser cavity is then optimised to correct the error.

In the laser cavity, errors are corrected by the use of a piezo electric mounted mirror, the tweeter, and a galvo driven brewster plate, the woofer. The tweeter is used to remove high frequency jitter of the laser. It has a 1 GHz correction range and 10 kHz frequency response. The woofer is used for low frequency changes, as when the laser is scanned. Both the tweeter and the woofer have gotten their names from Hi-Fi terminology.

The system might seem fail-proof but the Fabry Perot is the failing part. This is supposed to be a stable reference but temperature changes in the room affects it and makes the laser drift in frequency. A supplementary external reference is needed. Since the internal stabilisation system also affects the linewidth of the laser (reduces it to 1MHz) it can not easily be replaced by another system. The short time stability of the laser is thought to be enough without external stabilisation so it is only the longtime drift that should be adjusted. The external system should not be faster than the tweeter, to make sure that resonance is not produced in the system. The external system is connected to the laser by using the external frequency scan input on the laser control box. This makes a brewster plate in the Fabry-Perot tilt, changing the fringe pattern, and thereafter the internal system in the laser will follow, changing the frequency.

2.7.3 Frequency Modulated Saturation Spectroscopy

By looking back at the formulas 2.4, 2.7 and section 2.5 it is clear that those can be combined to produce frequency modulated saturation spectroscopy of Iodine. In such an experiment the set-up is more or less the same as in section 2.5.3. The pump is here frequency modulated and will make the detected probe have the form of the derivative of the absorption profile.

The Experimental Set-up

To produce the frequency modulated signal two AOMs are used. The beam that is to be modulated is focused on the first AOM. The AOM produces beams of many orders and the +1 order is chosen with an aperture by blocking all the other orders. A lens is placed after the aperture with the AOM in its focal point. This AOM turns the first order beam and it is focused on a second AOM by the lens. Also here the first order beam is selected and by putting a lens it retrieves its original Gaussian profile, as in figure 2.7

The AOMs are frequency modulated by connecting a function generator serially with the stable voltage source deciding the frequency of the AOM. Adjusting the frequency of the function generator changes the modulation frequency. In order to make the approximation with only the zero and plus-minus one orders of the Bessel functions in section 2.1.3 the amplitude of the sinusoidal signal of the function generator ought to be low.

After the AOMs the pump beam is directed through the Iodine cell. To make a good overlap between the pump and the probe beam, two apertures are installed. They are put approximately 1m apart, one at each side of the Iodine cell. The aperture opening is about 1mm. Each beam will now have a directional accuracy of 1mrad, giving the overlap a precision of 2mrad. To increase this precision the distance between the apertures need to be increased. This however increases the space needed in the laboratory for the stabilisation set-up. The precision of 2mrad is good enough to find a signal, and afterwards optimisation is possible without the apertures.

The probe beam has an intensity of about 10% of that of the pump, is directed in the opposite direction through the cell. After the cell it is reflected by a beamsplitter, directing it to a detector. The signal from the detector is filtered at the modulation frequency by a lock-in amplifier.

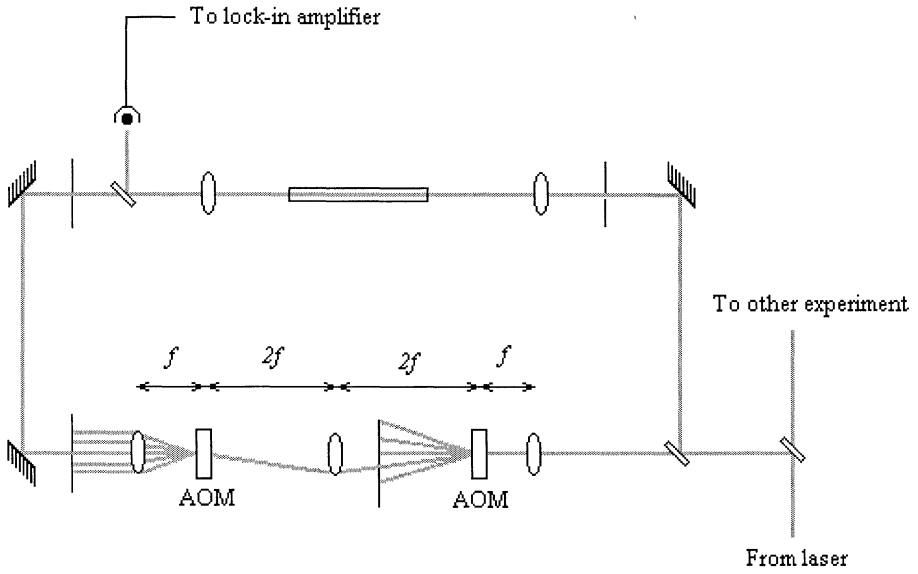

Figure 2.7: The principles of the experimental set-up for the frequency stabilisation experiment.

The optical part of the experimental set-up can be seen in figure 2.7.

Detection of the Frequency Modulated signal

In the ideal case the intensity in formula 2.7 is the transmitted intensity of the pump. This intensity gives information about the derivate of the absorption profile of the media. Since the gas is Doppler broadened this information will be drowned in the Doppler profile.

The non-transmitted intensity will then be absorbed by the gas. As in section 2.5.3 a probe beam going in the other direction through the gas will give information about the sub-Doppler profile. When the absorption is not saturated in the gas the depth of the hole will, according to formula 2.5.2, be linearly dependent of the intensity. This will then give a hole in the absorption profile proportional to $1 - I_t$, where I_t is the transmitted intensity in formula 2.7. The transmitted signal form the probe is proportional to the hole depth and will be of the form

$$\begin{aligned} I_{probe} \quad \propto \quad & 1 - A * exp(-2\alpha_0)[1 + (\alpha_{-1} - \alpha_1)\beta cos(2\pi\nu_{FM}t) \\ & +(\phi_1 + \phi_{-1} - 2\phi_0)\beta sin(2\pi\nu_{FM}t)], \end{aligned}$$

where A is a constant describing the intensity of the pump and the change in susceptibility at this intensity. $\alpha_{-1,0,1}$ is the absorption at the fundamental frequency and the two sidebands. In the same way $\phi_{-1,0,1}$ describes the dispersion. Since the whole probe beam is always detected, the dispersion effect is not treated.

The lock-in amplifier detects a derivate of the absorption profile as the laser is scanned through the absorption profile of the laser. The lock-in amplifier will, as seen in section 2.1.4, detect the signal $\alpha_{-1} - \alpha_1$ which is the difference in

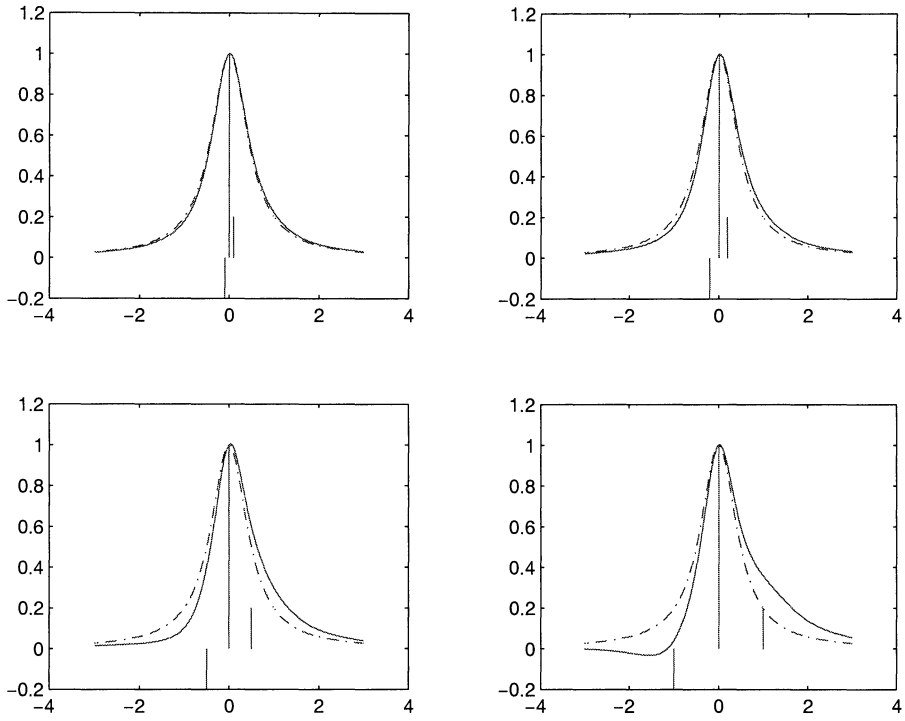

Figure 2.8: Three Lorenz profiles, one for each frequency component of the laser, are added. The dashed line is the non-modulated Lorenz profile of the laser. The vertical lines are the centered main frequency and the two first sidebands. The profiles are normalised so that the maximum is 1 and the FWHM is 1MHz. In the top left image a frequency modulation, in the same order as used in this thesis, of 100kHz is added. Hardly any change of the frequency profile is visible. In the top right image the modulation is 200kHz, the lower left 0, 5MHz and lower right 1MHz. Not until the modulation is of the same order as the linewidth of 1MHz a change of the line profile is visible.

absorption of the two sidebands. When the laser is scanned the sidebands will work their way over the absorption profile and thus the difference between the two is proportional to the derivative of the structure.

In this thesis the laser bandwidth was 1MHz and the modulation frequency was $50 - 100$kHz, limited by the lock-in amplifier. The modulation depth, i.e. β in equation 2.1, which describes the maximum deviation from the non-modulated frequency was on the order of $2, 7$MHz.

In the ideal case, when a hole was burnt, a very clean frequency profile could be found. In the experiments, however, the profile did not change much, as can be seen in figure 2.8. The top-left image is the simulated modulation situation with the equipment used for this thesis. The detected absorption profile of the gas does not change much since the main properties of the modulated laser line profile are preserved, the result is a suppressed signal.

The very large modulation depth will as well suppress the signal. When β is large the approximation of only two sidebands done in section 2.1.3 is

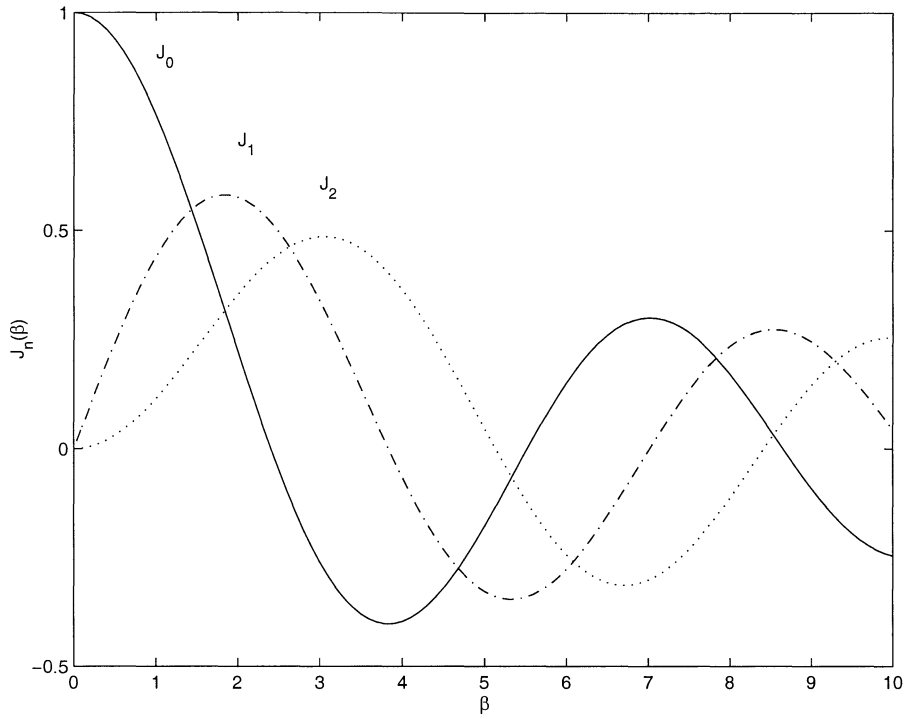

Figure 2.9: The first three Bessel functions.

no longer valuable. Many sidebands placed around the main frequency at the distance ν_{FM} from each other. Even orders of the sidebands will be symmetrically placed around the main frequency and odd orders antisymmetrically as $J_{-n}(\beta) = (-1)^n J_n(\beta)$. Those higher order sidebands will destroy the former clean profile since beating between different orders of sidebands, separated by ν_{FM} will be detected by the lock-in amplifier. The amplitude of the first 3 Bessel functions are plotted in figure 2.9. Viewed in the time-domain the frequency modulation will cause the frequency of the pump to oscillate. As long as the frequency oscillation amplitude, β is kept at the size of the laser linewidth the lock-in will always have a signal to measure. In this thesis the laser linewidth is 1MHz and the modulation depth is almost 3MHz. This essentially means that the lock-in will have heavily reduced signal strength.

2.7.4 Feedback System

The lock-in amplifier will help detect the hyperfine structure of Iodine. When the laser frequency is scanned over some absorption lines the frequency modulated detection system will produce a derivative of the absorption spectra in Iodine. This information is used as an error signal. In figure 2.10 (b)-(d) a zoom-in is done on single hyperfine lines of a frequency scan of 500MHz as seen in (a). Compared to the spectra in figure 1.7 this one, in figure 2.10 (a) might seem very noisy. The latter one is however made under more realistic forms, where the wavelength of the laser is chosen to fit the absorption profile of crystals used for the quantum computer and single-photon echo projects. In

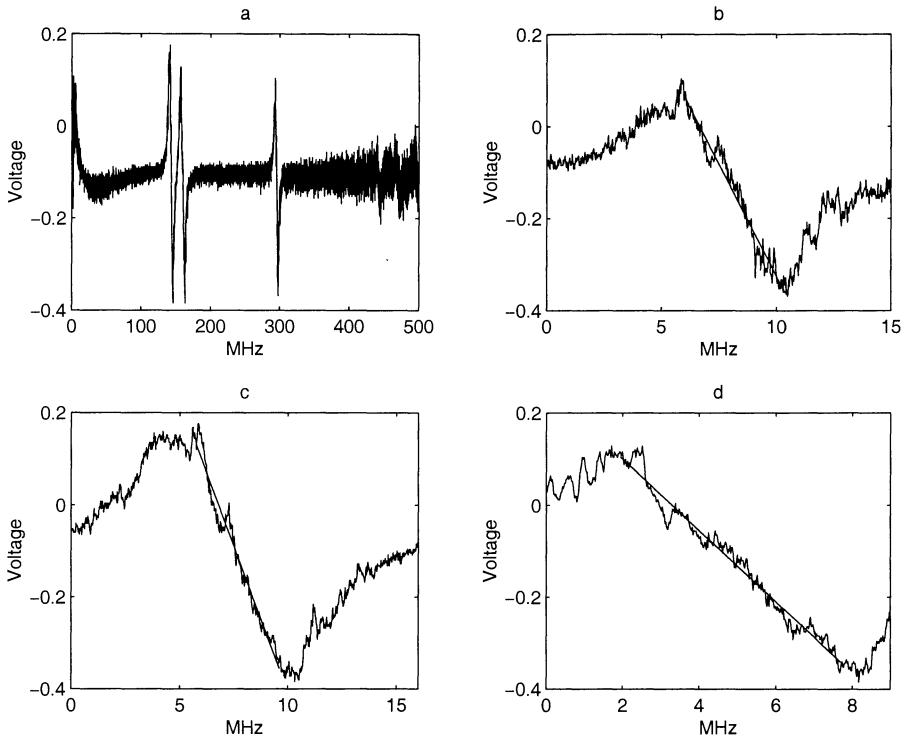

Figure 2.10: A zoom-in on one hyperfine level in Iodine is done to determine the ration between the frequency and voltage at the center of the line. In (a) the whole laser scan of 500 MHz at the wavelength 605, 784nm is recorded and three hyperfine levels are detected. In (b) the single isolated hyperfine level in (a) is zoomed, in (c) the left and in (d) the right of the pair. All the lines have a slope in the interval $70 - 130$mV/MHz at the line center.

figure 1.7 the laser is scanned through all of its frequency range until a strong fluorescence line of Iodine is seen. When recording the spectra in figure 2.10 the wavelength of the laser was 605.784nm, suited for the $Pr : Y_2SiO_5$ crystals. This is far from the peak of the Rhodamine 6G dye so the output intensity of the laser is greatly reduced. The last big difference between the two spectra is that in figure 1.7 a large time constant in the lock-in amplifier is used to reduce the noise and produce a beautiful spectra. In figure 2.10 the time constant is set as low as possible, not to interfere with the measurement of the hyperfine line properties.

In figure 2.10 (b), (c) and (d) a straight line has been adapted to the mid part of the hyperfine line. With this straight line approximation the relation between the frequency and voltage is easily found. For the three lines plotted it is

(b) 97mV/MHz

(c) 127mV/MHz

(d) 78mV/MHz.

By changing the sensitivity, i.e. the amplification, of the lock-in amplifier this result can be changed by many orders. The important thing here is that all the lines tend to have approximately the same properties at their midpoint.

Since the thermal noise in cables tend to be about 1mV the ratio in V/MHz was raised to about 1V/MHz by increasing the amplification in the lock-in. Without this increase the signal required to achieve the desired stability of 100kHz would lie within the noise and therefore would not be possible to achieve.

To compensate for the drift a specialised integrator circuit was constructed. An input error signal, called U_{in}, of 100mV is supposed to tell the laser to compensate 100kHz in frequency.

On the laser control box there is an input for external control of the laser frequency. This input is designed for a signal of $\pm$5V corresponding to the complete frequency scan interval of the laser. The scan should be kept low to increase the input resolution. It should also be kept high if a long time scale stability is desired. If the laser frequency drifts enough to make the hyperfine level used for locking go outside the scan interval the stabilisation will no longer work. To satisfy both criterias a scan interval of 500MHz is chosen. With this interval the hyperfine level would theoretically stay inside for hours. Since the laser mode-hops at least once every hour this should be large enough. It is also good to be able to have multiple hyperfine energy levels within the interval. This makes it possible to change frequency without interfering too much with the laser when the studied material gets worn out at a specific frequency. A worn out frequency is when long-term structures are burnt into the absorption profile and new experiments are difficult to perform because there are no ions left in the crystal to absorb at the frequency.

A frequency scan interval of 500MHz will give an input resolution of

$$10\text{V}/500\text{MHz} = 2\text{mV}/100\text{kHz}.$$

This is still slightly higher than the background noise of 1mV.

With the signal sent to the laser control box is called U_{out}, the stabilisation unit can be simplified to an integral

$$U_{out} = k \int U_{in} dt. \tag{2.19}$$

It was desired to have the integrator to compensate for a 100kHz error within 2ms. The output should then be 2mV which gives a $k = 10/\text{s}$. To be able to optimise the equipment k is chosen to be changed with a logarithmic scale within $0,5 < k < 25$.

The electronics was designed by the electronic workshop and the circuit description can be found in figure B.1. The capacitor marked X is easily changed. By changing it, the amplification k and the integration time will change. These two variables are not separable since one is the inversion of the other. Small changes of k are achieved by turning the logarithmic knob placed on the front of the circuits box, changing the 100k-log resistance in the circuit. Large changes are done by changing the capacitator completely. By empirical lab work it was found that the capacitator needed to be changed from the original value. It was therefore changed from 30 to 1,5pF, decreasing the amplification a factor 20 and increasing the time constant by the same factor.

2.7.5 Stability Results

The frequency stability of 100kHz was not achieved at desired frequencies during this thesis. When the frequency could be chosen freely, and strong fluorescence lines in Iodine could be used, the error signal from the lock-in amplifier indicated a maximal deviation of 100kHz. Due to difficulties running the laser the evaluation of the stabilisation unit was not satisfactory. When the laser worked without too frequent mode-hops a stability within $\pm$1MHz was easily achieved at the wavelength 605.784nm. At short time constants for the integrator the laser frequency oscillated very fast leaving it out in the extreme points of $\pm$1MHz for most of the time. At long time constants the laser seemed to stay very still for 90% of the time, making fast tours to $\pm$1MHz the rest of the time.

The system was tested in two ways. A photon echo experiment was done with strongly attenuated writing pulses (see section 1.1.1) and a hole burning experiment where the hole position was followed.

In the photon echo experiment it should have been possible to accumulate for a longer time, producing an increase in the output signal by writing the same interference pattern in the crystal with every pulse train. If the laser drifts during this process two pulse trains might interfere destructively with each other erasing the interference pattern. The stability requirements was supposed to be within 10MHz. The stabilisation did however not give any increase in signal and the question about the stability requirement is evaluated at the moment.

The hole burning experiment was done to verify the locking. The result was, as mentioned above, a stability within $\pm$1MHz. Unfortunately we failed to record any data from this experiment. The unlocked laser drift was earlier measured and compared to a prototype for the stabilisation equipment. A hole is burnt and followed for minutes with the laser stabilised by the internal stabilisation system in figure 2.11 and by the external prototype system in figure 2.12. The extreme points in the holes gives the position for the hole in the comparasion made in figure 2.13.

Clearly the laser has become much more stable with the external stabilisation unit connected. It is also easy to use the system as long as the laser light does not change direction. If the laser changes direction the probe and pump beams will no longer overlap and no signal will be detected. As the system is placed close to the laser this effect is negligible. While testing the system with a different laser the beam was lead approximately 5m through the laboratory before entering the equipment. This resulted in lots of work trying to get any signal at all due to directional changes occurring when the laser was adjusted.

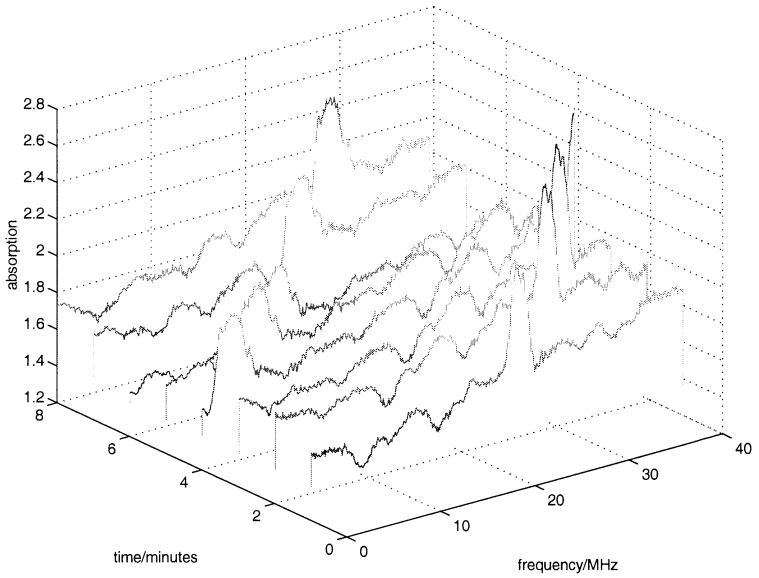

Figure 2.11: The laser drift on a short time scale without the external stabilisation. A hole is burnt in the absorption profile of $Eu^{3+} : YAlO_3$ crystal and read out every minute. After four minutes the hole disappears from the frequency interval and another hole from an earlier experiment appears in the other end of the interval. After four more minutes this old hole has passed the midpoint of the interval. This drift is comparable to what happened to the laser after 1,5h in figure 1.1.

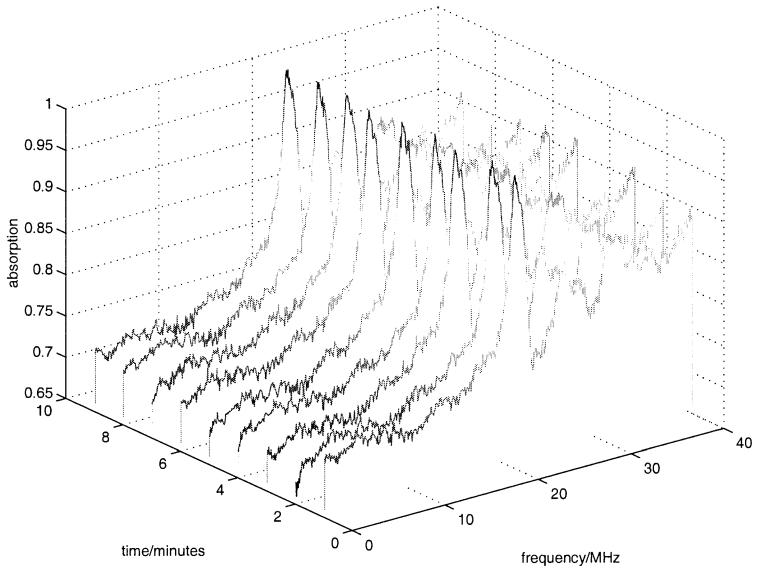

Figure 2.12: The same experiment as in figure 2.11 is made with an early prototype of the stabilisation system. The hole is much more stable than in figure 2.11. This early system worked for short time locking at Iodine hyperfine levels but was in general hard to maneuver.

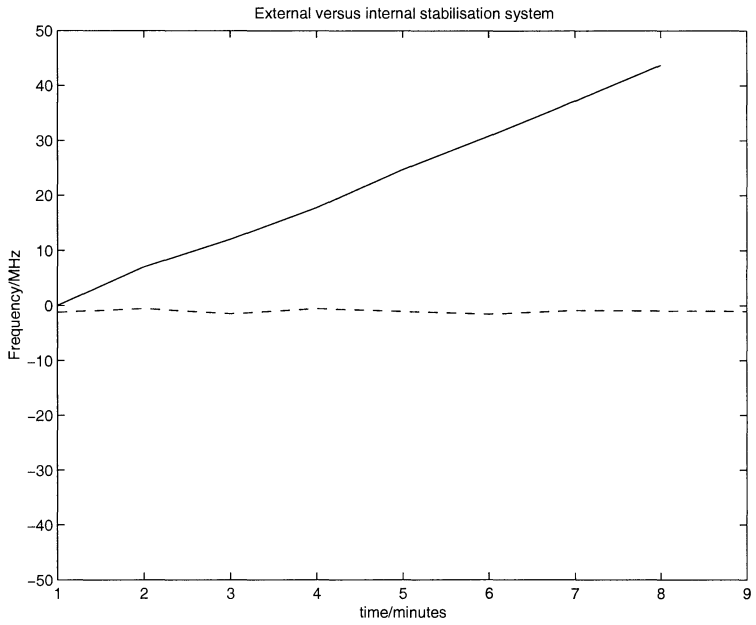

Figure 2.13: By taking the maximum of the holes in figure 2.11 and 2.12 a comparasion can be made. The dashed line is the externally stabilised system end the solid line is the internally stabilised system. The system becomes much more stable after locking on a hyperfine energy level of Iodine.

Chapter 3

Frequency shift

3.1 Introduction

Some experiments in the quantum-computing project were possible to fit in to this thesis. The experiments were to evaluate the level of ion-ion interaction in a $Pr : Y_2SiO_5$ crystal. The ion-ion interaction is, as described in section 1.1.2, a shift in resonance frequency of some dipoles due to excitation of others and is later supposed to be used to create entanglement between ions in the implementation of a C-NOT gate. The effect is based on that the Pr ions in the crystal have slightly different electric dipole moments at different energy levels. By exciting one dipole (Pr ion), all ions nearby will, because of the change in the local electric field, shift their frequency. For the construction of a quantum gate, knowledge about the shift in different materials is essential. Many materials and doping concentrations need to be examined to be able to produce a competitive quantum gate.

3.2 Experiments

3.2.1 Basic Principles of the Experiments

These experiments were performed on a short time scale, making it unimportant if the laser was locked or not. Also, since a large number of holes were burnt in the crystal the laser frequency had to be altered between every experiment, to let the material rest so that the burnt structure disappeared.

The experiments evaluate the amount of shift at a certain resonance frequency as a function of the excitation level at another frequency. Consecutive experiments of two main types were performed. In both cases a narrow hole was burnt in the absorption profile, and then excitation was done in another frequency region. Afterwards the hole was read and properties as the full-width-half-maximum (FWHM) and height of the detected hole were calculated from the data.

In the first experiments the output power, while exciting dipoles at a different frequency interval, was constant. The size of the frequency interval was altered. Seven different frequency intervals were tried logarithmically spread between 0 and 77MHz with many measurements on small intervals and few at high ones.

In the second experiment the excitation frequency interval was kept constant at the maximum of 77MHz. In this experiment the excitation power was changed. The AOMs used have a specific voltage that should activate them. According to the manufacturer they are discrete, transmitting zero or full power, which is not true. By slowly increasing the voltage for the AOMs an increase of the transmitted power can however be achieved in a controlled way.

In both experiments the read-outs are cycled. For example in the first experiment the cycle is that first the hole is read out once with no excitation, then with 2,6MHz, 5,1MHz,..., 78MHz. When all the excitation length from 0 to 78MHz have been read out the measurement restarts with no excitation and the cycle goes on 20 times. The big advantage with this cycled measurement is that changes like the laser frequency and output power will not affect the measurement in any systematic way. The noise in general will be reduced with more statistical data.

3.2.2 Experimental Setup

In the experiment AOMs were used to scan the laser frequency. AOMs should be used in pairs to avoid change in beam direction when the AOM properties are changed. The same technique as in section 2.7.3, figure 2.7, two AOMs are put in series with a lens in-between to invert the change in the beam direction by the first AOM. Two apertures are introduced, one between the AOMs and one after, to sort out the desired orders.

No interference should occur between the burnt hole and the excited area, only interaction arising from frequency shifting. If the excitation region and the hole are very close in frequency, effects like side structures from the excitation, can be introduced in the hole. This affects the result of the experiment by giving false values of the hole width and height.

A solution to the problem above is to use two different sets of AOMs for the hole burning pulse and for the excitation pulse. The AOMs will then be directed so that they shift the frequency in different directions. This can be done by introducing a beam splitter before the first AOM, steeling some of the laser power, or as done here by using the zero order beam passing through the first AOM, see figure 3.1. The zero order will go through two other AOMs, shifting the frequency in the opposite direction as for the first two AOMs.

Whatever method is used the beams have to be spatially overlapped after the AOMs. If the overlap is not good then the two beams will not communicate with ions in the same spatial region. The interaction effects we are looking for decrease with r^3 so overlapping is crucial.

The complete set-up for altering the laser beam intensity and frequency is shown in figure 3.2. To control the AOMs and to record the spectrum some electronics are also needed. Computer-controlled pulse generators produces pulses as in figure 3.3. Pulse (a) burns a hole in the absorption profile. This hole is later read by pulse (c), controlled by the same AOM-pair so that the writing and reading of the hole is at the same frequency. Pulse (b), which is controlled by another AOM pair, shifting the light in the opposite direction, excites atoms in another frequency interval, far from the hole.

In the first experiment the length of pulse (b) is changed and in the second experiment changes are done to the amplitude. Pulse (a) and (c) are the same in both experiments.

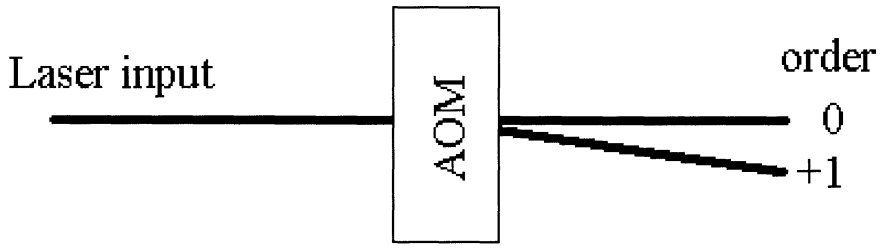

Figure 3.1: When the AOM is turned on, the first order deflection is used and when it is off the beam traverses the AOM unchanged. The-non altered beam can then be used for other experiments without any power losses caused by the alternative experimental design were the second beam is achieved with a beam splitter.

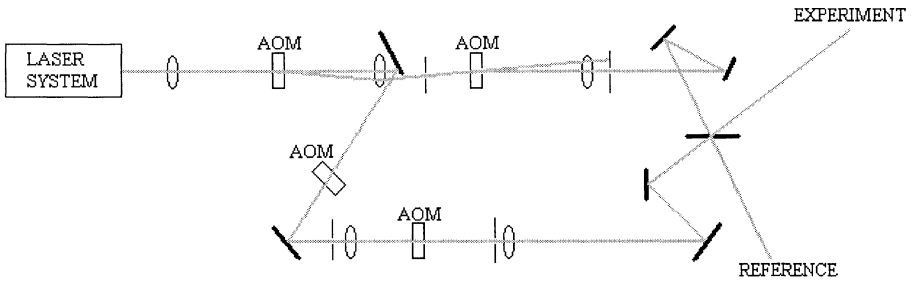

Figure 3.2: The experimental set-up for the frequency shift experiments. In the two AOMs in the top of the figure the frequency is shifted in one direction, opposite of that of the other two AOMs. This way an experiment with a large separation between hole and excitation frequencies can be performed.

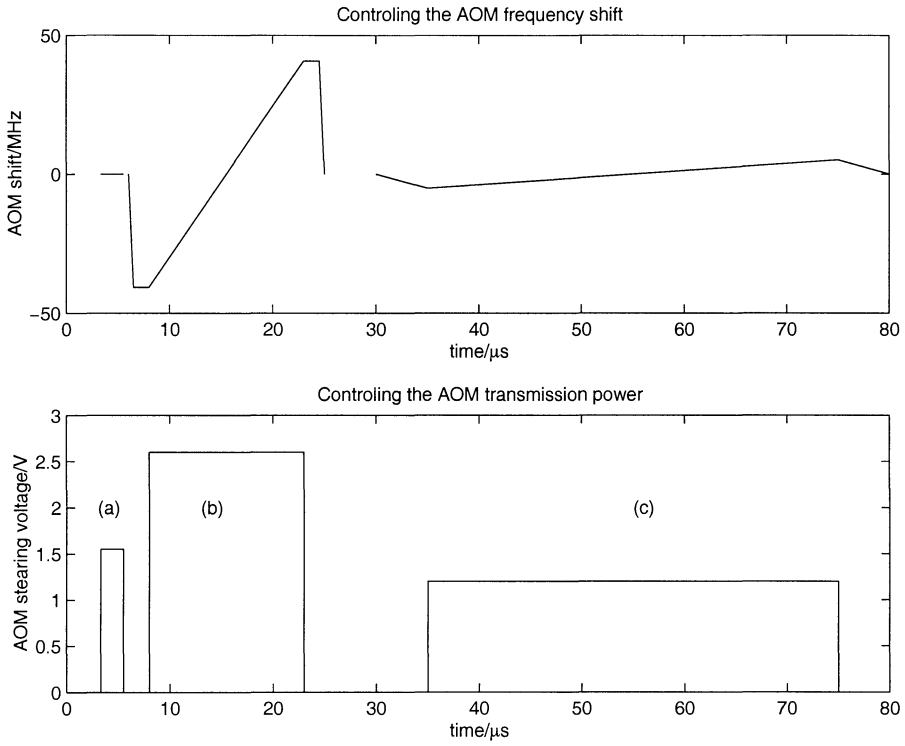

Figure 3.3: The frequency shift (upper) and transfer power (lower) through the two AOM sets used for the experiment. Pulse (b) is controlled by another AOM pair than (a) and (c). The frequency zero level will then not be the same for (b) as for the others.

Dependence of Excitation Interval

By exciting different sized intervals in the frequency spectra a linear relation between the size of the excited interval and the amount of shift was expected. Only by doing one series of excitations with different intervals would not give any clearly visible results. The individual deviations are too large. By doing twenty consecutive measurements and performing an average the expected results should be detectable.

Two slightly different experiments were done. The basic principle was the same, the excitation interval started at zero and increased logarithmically to 78MHz. In one of the experiments the highest excitation frequency was fixed and the lower was changed, and in the other it was the opposite. The full excitation interval was the same for both experiments.

Dependence of Excitation Intensity

As in the interval dependence experiment above this experiment was performed repetitively to average out noise. This experiment consisted of exciting the full interval of 78MHz as above but with 21 different intensities. The recording intensity was also measured. To produce this intensity fluctuation the voltage opening the AOMs were changed with steps of $0,1$V, between $0,8$V and $2,8$V. The intensity transmission through the AOM is then S-shaped, as almost no intensity is let through for low tensions and almost all for high ones. The amount of shift was calculated as above and figures were produced to show the shift dependence of intensity.

Evaluation Procedure

Since the writing pulse was very short a $sinc^2$ is adapted to the curves without any excitation present at all (excitation interval is zero). The curve form is a direct result of Fourier analysis of the burning pulses, approximated to be delta-peaks.

When this has been calculated an average of the full-width-half-maximum (FWHM) is calculated to produce an average $sinc^2$ response. With the excitation present the hole is expected to undergo a Lorenzian broadening. A convolution between the $sinc^2$ and a $Lorenzian^2$ is fitted to every hole. Some holes with their fitted functions can be seen in figure 3.4.

The same procedure is used for calculating the shift at the experiment with different intensities.

3.2.3 Results and Discussion

The results of the different experiments are plotted in figure 3.5, 3.6 and 3.7. In all three experiments the basic principle is the same; by adding more excitation power, the shift is expected to increase linearly. The figures show a good relation between the hypothesis and the result. Figure 3.5 and 3.6 should theoretically express the same shift for the highest excitation interval since the two situations are equal in the experiments. However if the laser power has changed in-between the experiments, the amount of shift is changed.

In figure 3.7 a clear relation between the laser power and the amount of shift is shown. Unfortunately the detection of the transmitted power through the

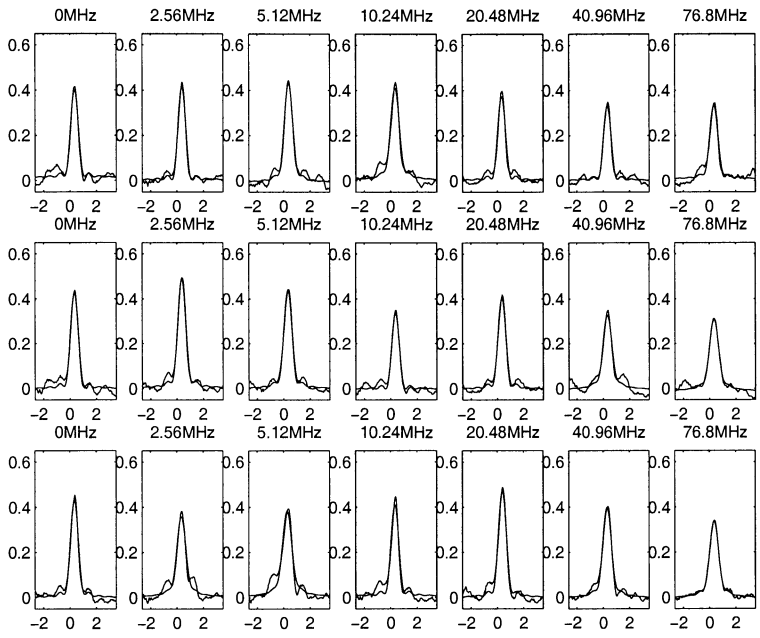

Figure 3.4: An example of curve-fits to the holes. The horizontal scale is in MHz and the left figures are all without any excitation on other frequency intervals after the hole burning. The excitation increases to a maximum at right figures.

AOMs was saturated during the experiment, as seen in figure 3.8. A dashed line is added to the figure as a realistic approximation for the power increase with the applied voltage on the AOM opening control. By adjusting for this error figure 3.9 can be produced. Comparing with figure 3.7 there is no longer a big pile of data around the transmitted power of $3,5$(arb. unit).

The shift has been compared with simulated data for the crystal. The amount of shift is what is expected for this crystal.

3.3 Future Improvements

This computer controlled measurement turned out to be a very powerful way of doing repetitive measurements. Without the averaging process this measurement would not be possible, and doing all those measurements by hand, without the help of a computer would take to much time.

This experiment was done with the laser scanning a wide frequency interval. Locking the laser wouldn't help this kind of experiment since old hole structures would be confusing for the calculations. Therefore this experiment would not be helped by the Iodine frequency locking earlier in this thesis.

Measurements could be done with other crystals with different doping concentrations. By measuring a wide range of crystals, it would be easy to find the best concentration for constructing a quantum computer.

By repeating the experiments a larger number of times a better statistical material would be obtained. Depending on the need for high precision this could be an important step. One experiment, measuring the frequency shift for

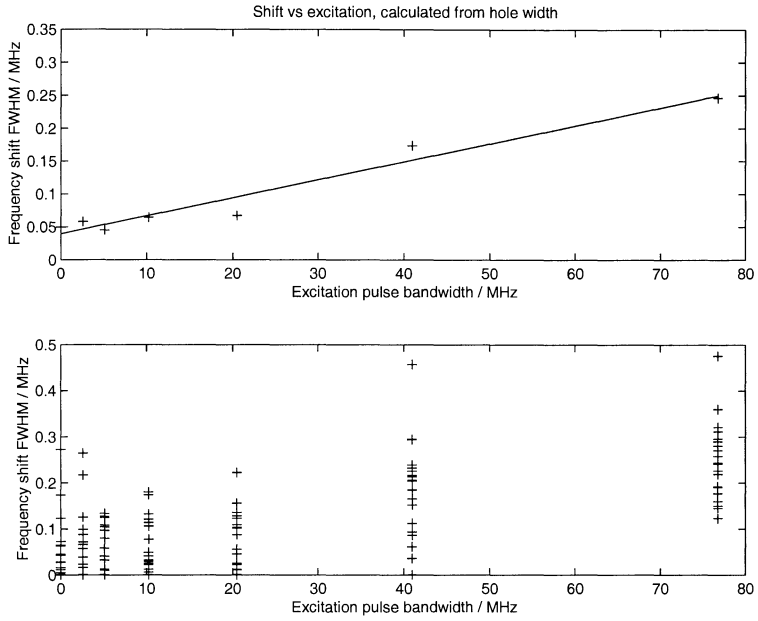

Figure 3.5: The amount of shift as a function of the excited frequency range. The higher figure is an average of the 20 different measurements in the lower figure.

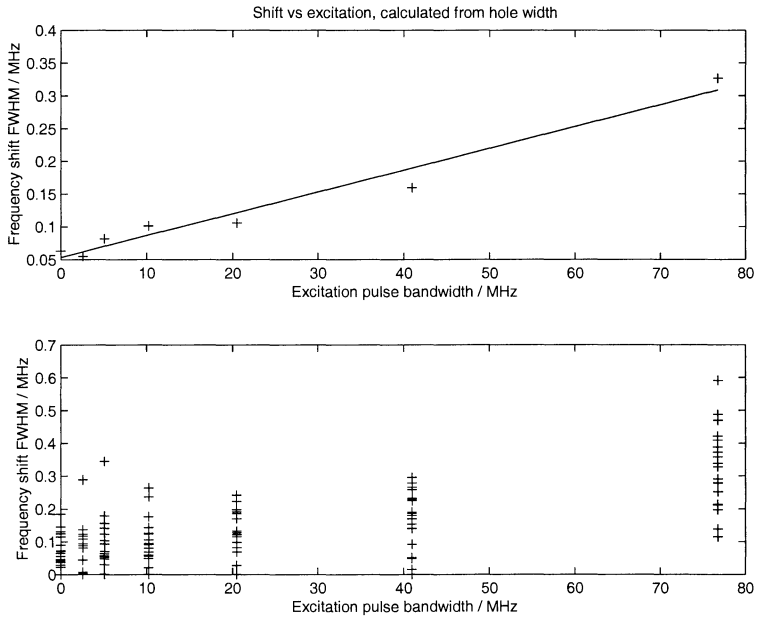

Figure 3.6: The amount of shift as a function of the excited frequency range. The higher figure is an average of the 20 different measurements in the lower figure.

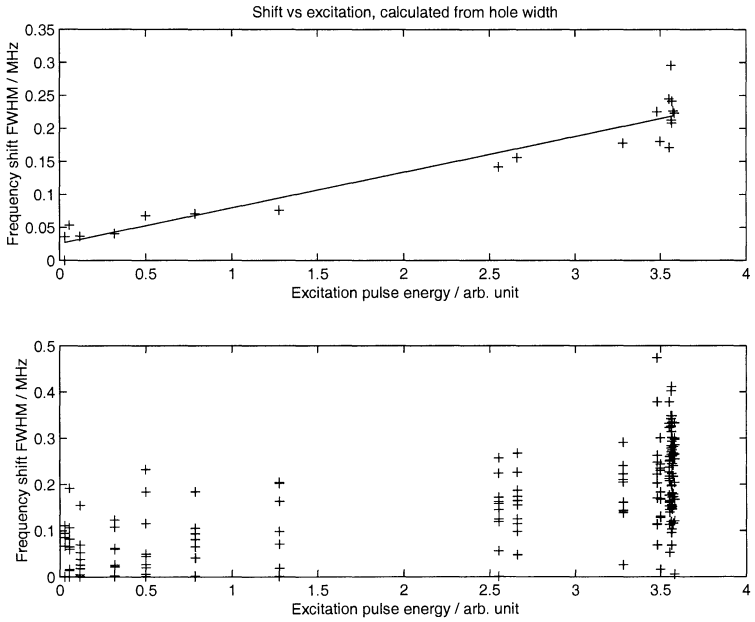

Figure 3.7: The shift versus the excitation power is plotted. In the upper figure an average is taken from the 10 measurements done at every transmitted power. The detectors got saturated at high powers, leaving a large pile of data at the right end of the figure. By adjusting the transmitted power in a realistic way, as in figure 3.8 this figure can be redrawn as in 3.9. Note that a plus in the none averaged figure can consist of many overlapped plus.

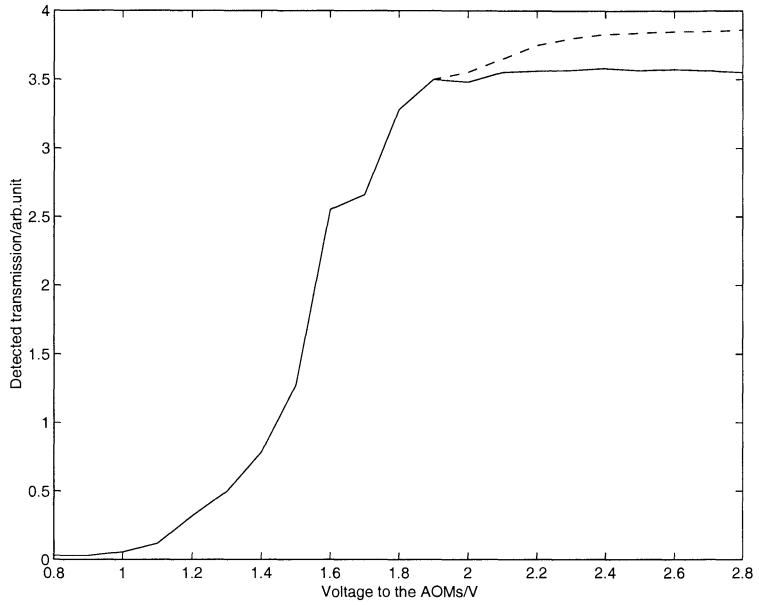

Figure 3.8: The transmission through the AOMs. By applying the voltage at the horizontal-axis, the AOM will transmit the power at the vertical-axis. The dotted line at the top is an approximation since the detector was saturated during the experiment, giving the sharp edge and not the S-shaped curve that was expected.

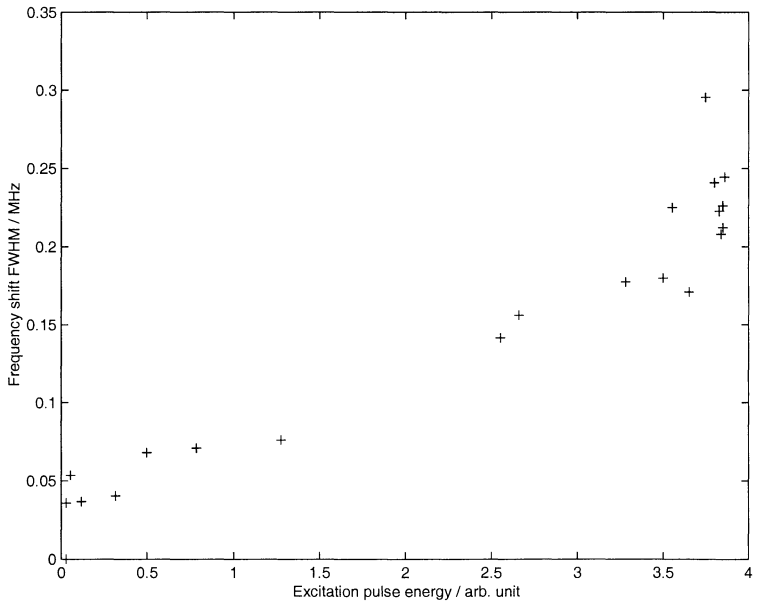

Figure 3.9: In this figure the transmitted power through the AOMs has been adjusted. The big pile of measurements at higher powers in figure 3.7, were the detector was saturated, is now stretched out in a realistic way.

7 different excitation intervals and averaging for 20 measurements, took approximately 40 minutes to perform. When knowing what to look for a doubling of this time, i.e. a doubling of the amount of data, or the amount of measuring-points, would indeed be possible.

In this experiments two AOMs were used for the excitation frequency scanning. By adding two more AOMs a frequency interval of twice the size could be scanned and larger shifts to be observed.

Chapter 4

Conclusions

As Dye-lasers are the only really good alternative, as a tuneable continuous laser in the visible range, work has to be done on improving their properties.

The two Coherent 699-21 laser systems used in the Photon Echo group, at Lund Institute of Technology, were constructed in the late seventies and early eighties. More modern models of the lasers do not improve the properties enough to justify changing the systems. The major improvements through the years have been upgrading the pointing stability of the pump lasers and to increase the pump laser power.

The stabilisation scheme that has been tested in this thesis (section 2.7) has been implemented to adjust for long-time drifts of the laser. The hope for this system was that it should be able to reduce the long-time drift to zero without affecting the laser frequency bandwidth. This, however was a task much more difficult than first thought.

As stated in section 2.7.5 the laser stops drifting with the system installed. The laser properties are however changed as the frequency oscillates around the locking frequency. The same scheme has been implemented by many other groups in the world and their official result are better than the ones obtained in this thesis. Possible reasons for that has been discussed in section 2.7.5.

The long time stability of the laser is not the only improvement wanted for the laser. A decrease of the laser bandwidth is also desirable, in experiments as the ones in chapter 3, in order to be able to burn narrow holes in the absorption profile. To implement this the internal stabilisation of the laser must be overrun. A system of this type, where the laser is locked to a hole in the absorption profile of the crystal (see section 1.2.2), used for the quantum computing and single photon echo experiments, is currently evaluated by Lars Rippe, PhD student in the group. The goal is to lower the frequency bandwidth of the laser to $10kHz$ in combination with no long-time drift. This system should be working in approximately one-years time.

Even with the laser frequency locked there are more features to be improved on the laser. When controlling the qubits in the quantum computer scheme described in section 1.1.2, exact π-pulses are to be used. To produce this the laser output power must be known. Very simple tests were performed for this using the electric circuit in figure B.1. The Laser light had to pass through an Electro-optic modulator, that turned the polarisation of the light and a polarisation filter, as a reference. Adjusting the off-set of a photo diode signal

so that a zero signal is achieved at the desired intensity of the laser light that was transmitted through the EOM and the polarisator, gave fairly good intensity stability when integrating and sending feedback to the EOM. The electronics, i.e. the integrators time constant etc., used were however not at all adapted for this system, introducing small resonance oscillations of the intensity.

Except for the improvements in the laser, computer-controlled measurements have been used for the frequency shift experiments in chapter 3. This turned out to be a very powerful way of gaining a wide statistic material in an experiment. It would be advisable to develop a suitable interface in Labview for the quantum computer experiments. At the present time modifications in the program code have to be done for every new experiment. The development of such an interface might be a good proposal for another master's thesis in the group.

Acknowledgements

This report is the end of 6 years of university studies. There are many people to whom I owe great thanks during these years. It would be impossible to name you all.

To some people in the Atomic Physics Division in Lund I owe my gratitude for all the help and support on the way to this report. First of all, my supervisor Stefan Kröll, who took me in and helped me in all different ways. Thank you also Lars Rippe, Nicklas Ohlsson and Mattias Nilsson, the three PhD students in the group, thanks for giving me some of that knowledge you possess. For all your help I would like to thank Markus Persson, former diploma worker in the group. The last two, for outsiders unknown, members of the group, Blyger and Toker deserve special thanks for not being too stubborn when it comes to lasing.

In the Atomic Physics Department there are also many other people that needs a special thank you. Tomas Christiansson and Ola Synnergren for cheerful chats and good advise at lunch and tea-time. Thank you Åke Bergquist for all the help with the electronics.

For all of you that have read my report and have given constructive critics about it, I couldn't have done it without you.

For all my friends and my family, thank you for your support and for not turning the back on me in difficult situations.

Bibliography

[1] Tomas Christiansson
A first step towards Quantum Computing in Rare-earth-ion-doped crystals
Master's thesis, **LRAP-266**, Department of Physics, Lund Institute of Technology, Feb 2001.

[2] Nicklas Ohlsson, R. Krishna Mohan, Stefan Kröll
Interference between non-overlapping wave-packets of a single photon
Conference digest 2000 International Quantum Electronics Conference, page 122, Nice France 10-15 Sept 2000.

[3] A. E. Siegman
Lasers
University Science Books, Mill Valley, California 1986.

[4] Nicklas Ohlsson, R. Krishna Mohan and Stefan Kröll
Quantum Computer Hardware based on Rare-earth-ion doped Inorganic Crystals
Optics Communications **201**, 71-77, Jan 2002.

[5] P. B. Sellin, N. M. Strickland, J. L. Carlsten and R.L. Cone
Programmable frequency reference for subkilohertz laser stabilisation by use of persistent spectral hole burning
Optics Letter **24**, 1038-1040, Aug 1999.

[6] Gary C. Bjorklund
Frequency-modulation spectroscopy: a new method for measuring weak absorption and dispersions
Optics Letter, **5**, No 1, page 15, Jan 1980
IBM Research Laboratory, San Jose, California.

[7] Ulf Gustafsson
Diode laser spectroscopy in extended wavelength ranges
PhD, **LRAP-253**, Department of Physics, Lund Institute of Technology, Apr 2000.

[8] Peter Kauranen
Near-Infrared Diode Laser Frequency-Modulation Spectroscopy for High-Sensitivity Gas Analysis
PhD, **LRAP-185**, Department of Physics, Lund Institute of Technology, 1995.

[9] Gunnar Sparr, Annika Sparr
Kontinuerliga System
Studentliteratur 1999.

[10] Stanford Research Systems
Model SR510 Lock-in Amplifier, users manual.

[11] Young, Freeman
University Physics
Ninth edition, Addison Wesley 1996.

[12] Sune Svanberg
Atomic and Molecular Spectroscopy, Basic Aspects and Practical Applications
Second Edition, Springer 1997.

[13] Göran Jönsson
Atomfysikens Grunder, del ett & del två
Teach Support, Lund 1997 & 1996.

[14] Claude Cohen-Tannoudji, Bernard Diu, Franck Laloë
Mécanique quantique II
Hermann, 2000.

[15] G. Herzberg
Spectra of Diatomic Molecules
Van Nostrand Reinhold Company, New York, 1950.

[16] Anders Persson
Laser Spectroscopic Techniques Applied to the Study of Excited States of Free Atoms, Ions and Molecules
PhD, **LRAP-116**, Department of Physics, Lund Institute of Technology, 1990.

[17] T. W. Hänsch, I. S. Shahin, A. L. Schawlow
High resolution saturation spectroscopy of the sodium D line with a pulsed tunable dye laser
Physical Review Letters **27**, 707, 1970.

[18] Christian Bordé, Alfred Kastler
Spectroscopie d'absorption saturée de diverses molécules au moyen des lasers à gaz carbonique et à protoxyde d'azole.
Comptes Rendus Hebdomadaires des Séances de l'Académie des sciences **B271**, page 371.
Gauthier-Villars, Paris, 1970.

[19] G. C. Bjorklund and M. D. Levenson
Sub-Doppler frequency-modulation spectroscopy of I_2
Physical Review A, **24**, 166-169, Jul 1981
IBM Research Labratory, San Jose, California.

[20] J.L. Hall, L. Hollberg T. Baer, and H. G. Robinson
Optical heterodyne saturation spectroscopy of I_2
Appl. Phys. Lett. **39**, 680-682, 1981.

[21] N. H. Tran, R. Kachru, P. Pillet, H. B. van Linden van den Heuvell, T. F. Gallagher, and J.P. Watjen
Frequency-modulation spectroscopy with a pulsed dye laser: experimental investigations of sensitivity and useful features
Applied Optics, **23**, No 9, 1353-1360, 1984.

[22] B. Couillad, A Ducasse
Refractive Index Saturation Effects in Saturated Absorption Experiments
Laboratoire Spectroscopie Moléculaire, Université Bordeaux I, France
Physical Review Letters **35**, 1276-1279, Nov 1975.

[23] C. Kittel
Introduction to Solid State Physics
Seventh Edition, John Wiley & Sons 1996.

[24] D. Cheng
Field and Wave Electromagnetics
Second Edition, Addison Wesley, 1989.

[25] E. Hecht
Optics
Second edition, Addison Wesley, 1987.

[26] Kristin Bjornsen
Frequency Stabilization of a Dye Laser using the Hyperfine Absorption Spectra of Iodine
http : //lamar.colostate.edu/~lasers/undergrad/iodine.htm

[27] Coherent
699 Dye Laser Users Manual.

[28] Spectra-Physics
Millennia Vs, Diode-pumped, cw Visible Laser, User's Manual.

[29] H. Hertz, L-Å. Nilsson
Konstruktion och testning av digital våglängdsmätare
Master's thesis, **LRAP-2**, Lund Institute of Technology, 1980.

Appendix A

Equipment

In this chapter the scientific equipment used in this thesis is described. Many specific properties of the equipment used is discussed in other parts of this thesis. For more information about the equipment reference is made to the user's manuals.

A.1 Laser System

The laser system is a Coherent 699-21 Ring Dye laser pumped by a Millennia Vs Diode-pumped, cw Visible laser. Other pump lasers have also been used during this thesis, but no one of them produced satisfying results.

A.1.1 Spectra-Physics Millennia Vs Diode-pumped, cw Visible Laser

Two high-power, fiber-coupled laser diode bars are used to pump a laser gain medium of neodymium yttrium vanadate, $Nd : YVO_4$. A lithium triborate, LBO, crystal is placed in the cavity to double the frequency to visible light of the wavelength 532nm. The maximal output power is 5W.

The diode bars are placed in the power-supply and the light is transmitted to the laser cavity by fibers. By doing this a lot of space for the experiment is saved on the laboratory table.

For more information about this laser see [28].

A.1.2 Coherent 699-21 Dye laser

This laser is standard equipment in many research facilities. It is a ring-dye laser pumped by a broadband fixed laser as the one described in A.1.1. The basic structure of the laser is shown in figure A.1. A small fraction of the output light is split off the main beam after the Output Coupler. This light is used for the internal stabilisation system of the laser. The stabilisation system is based on a temperature stabilised Fabry-Perot interferometer. The frequency fringes produced by the Fabry-Perot are used as error signals for the stabilisation unit. Those fringes will be dependent on the intensity of the laser, so another detector is used to record the intensity. To adjust for frequency changes in the

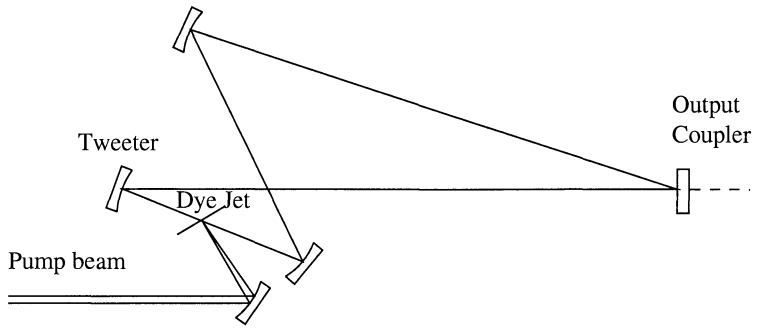

Figure A.1: The basic structure of a Coherent 699-21 Dye laser. The woofer, that adjusts for low-frequency changes of the laser frequency, is placed just before the Output Coupler.

laser output the length of the cavity must be adjusted. This is accomplished by translating a piezoelectric mounted mirror, called the tweeter, or by tilting a plate at the Brewster angel called the woofer. Both the tweeter and the woofer have gotten their names from hi-fi equivalents, since the tweeter adjusts for high-frequency gitter and the woofer for low-frequency errors. The internal stabilisation system will reduce the laser frequency bandwidth to 1MHz.

As seen earlier in figure 1.1 this laser system is not fail-proof. Without any other external stabilisation system the laser will frequency drift approximately 100MHz/h.

A.2 Signal Detectors

Hamamatsu, ***S1223*** Four, two by two identical, silicon PIN photo diodes with internal amplification. They are used with double-shielded matched coaxial cables.

A.3 Electronics

A.3.1 Factory Made Electronics

Stanford Research Systems, SRS DG535 Four-channel digital delay/pulse generator.
Stanford Research Systems, SRS DS345 30MHz digital arbitrary waveform generator.
Stanford Research Systems, SR510 Lock-in amplifier, see section 2.1.4 for further description.
Tektronix, TEK TDS540 Four-channel digitising 1GS/s oscilloscope.
Tektronix, TEK 2431L Two-channel digital 250MS/s oscilloscope.
Mascot, model 719 Power supply.
Hung Chang 8205A Sweep function generator.
ISOMET D322B Two acousto-optic deflector drivers.
ISOMET D1205C Four acousto-optic modulators, see section 2.1.3.

Bang & Olufsen SN17 DC power supply.

A.3.2 Locally Manufactured Electronics

Wavelength meter see [29].
DC Power Supply 28V, 800mA.
DC Power Supply 5V, 600mA.
Quad-high-speed Amplifier Amplification; 2-10, 2-10, 2-20 and 2-100.
Integrator

A.4 The Cryostat

A *CryoVac*150 cryostat is used to lower the temperature to 4K. This cryostat is essentially built up by two thermally isolated cylinders put inside each other. The studied sample is placed in the inner cylinder containing liquid helium. The liquid helium compartment is surrounded by vacuum to minimize thermal transport. To reduce the amount of used helium this vacuum compartment is placed in a bath of liquid nitrogen, isolated from the surrounding laboratory air by another vacuum compartment.

To have access to the sample the light must pass through three windows to reach the inner compartment.

If the pressure of the helium in the inner compartment is lowered by vacuum pumping, a temperature of 2K can be achieved. This option was not used during this thesis.

Appendix B

Technical Data

B.1 Drawing of the External Stabilisation Unit

To change the time constant/sensitivity of the circuit the capacitator marked X is changed.

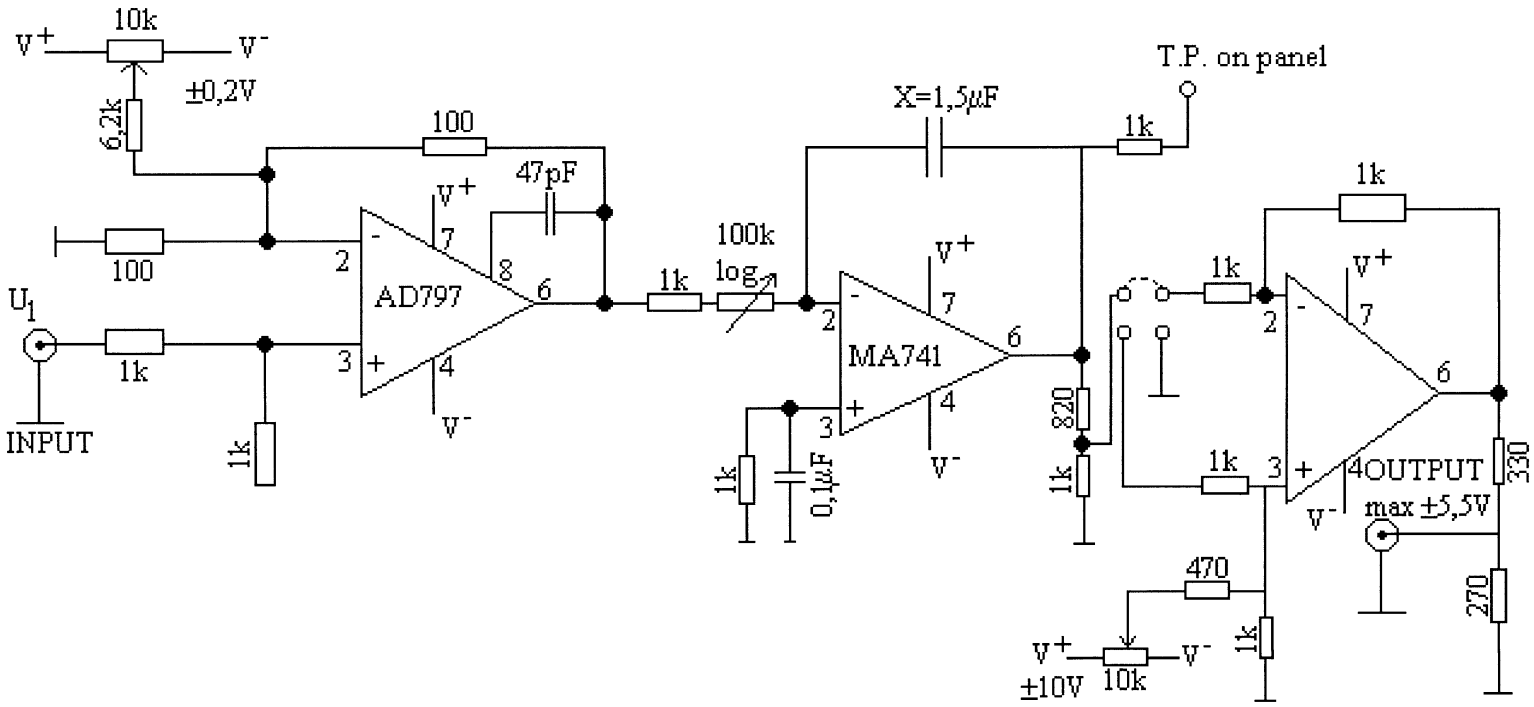
V+
10k
V-
±0,2V
6,2k
100
47pF
100
U1
INPUT
1k
AD797
2
3
7
8
6
4
1k
100k
log
X=1,5µF
MA741
1k
0,1µF
820
T.P. on panel
1k
1k
1k
1k
1k
470
±10V
10k
4OUTPUT
max ±5,5V
330
270